Passivity-Based Power Sharing and Voltage Regulation in DC Microgrids With Unactuated Buses

Albertus Johannes Malan, Pol Jané-Soneira, *Graduate Student Member, IEEE*, Felix Strehle, and Sören Hohmann, *Member, IEEE*

***Abstract*— In this article, we propose a novel four-stage distributed controller for a dc microgrid that achieves proportional power sharing and average voltage regulation for the voltages at actuated and unactuated buses. The controller is presented for a dc microgrid comprising multiple distributed generation units (DGUs) with time-varying actuation states, dynamic *RLC* lines, nonlinear constant impedance, current, and power (ZIP) loads, and a time-varying network topology. The controller comprising a nonlinear gain, proportional–integral (PI) controllers, and two dynamic distributed averaging stages is designed for asymptotic stability. This constitutes deriving passivity properties for the dc microgrid, along with each of the controller subsystems. Thereafter, design parameters are found through a passivity-based optimization using the worst-case subsystem properties. The resulting closed loop is robust against DGU actuation changes, network topology changes, and microgrid parameter changes. The stability and robustness of the proposed control are verified via simulations.**

***Index Terms*— DC microgrids, distributed control, passivity, power sharing, voltage regulation.**

I. Introduction

THE ADVENT of localized power generation and storage increasingly challenges the prevailing centralized power-generation structures. Originally proposed in [1], the microgrids paradigm envisions networks that can operate autonomously through advanced control while meeting consumer requirements. Although current electrical grids predominantly use ac, high- and low-voltage dc networks have been made technically feasible due to the continual improvements of power electronics. Indeed, dc microgrids exhibit significant advantages over their ac counterparts, demonstrating a higher efficiency and power quality while simultaneously being simpler to regulate [2], [3].

Manuscript received 26 May 2023; revised 4 December 2023; accepted 19 February 2024. Date of publication 12 March 2024; date of current version 25 June 2024. This work was supported in part by Germany's Federal Ministry for Economic Affairs and Climate Action [Bundesministerium für Wirtschaft und Klimaschutz (BMWK)] through the RegEnZell Project under Grant 0350062C. Recommended by Associate Editor V. Adetola. *(Corresponding author: Albertus Johannes Malan.)*

The authors are with the Institute of Control Systems (IRS), Karlsruhe Institute of Technology (KIT), 76131 Karlsruhe, Germany (e-mail: albertus.malan@kit.edu; pol.soneira@kit.edu; felix.strehle@kit.edu; soeren.hohmann@kit.edu).

Digital Object Identifier 10.1109/TCST.2024.3372308

In microgrids, power generation and storage units are typically grouped into distributed generation units (DGUs) that connect to the microgrid through a single dc–dc converter for higher efficiency [2]. This changes the traditionally centralized regulation problem in power grids into a problem of coordinating the DGUs connected throughout the microgrid. This coordination is generally realized as average or global voltage regulation in combination with load sharing between the DGUs (see [4], [5], [6]).

A. Literature Review

A vast number of approaches have been proposed for the voltage regulation and load sharing of dc microgrids, as detailed in the overview articles [3], [7], [8] along with the sources therein. These approaches are broadly categorized as either centralized, decentralized, or distributed in nature [3], [7], [8]. While centralized controllers can optimally coordinate the DGUs, they offer reduced scalability and flexibility and have a single point of failure [8]. On the other hand, decentralized controllers either only attempt to achieve voltage stability [9], [10], [11] or achieve load sharing at the cost of voltage regulation quality (e.g., the droop-based approaches in [3]).

In response to these limitations, numerous controllers for voltage regulation and load sharing that operate in a distributed manner have been proposed [4], [5], [6], [12], [13], [14], [15], [16], [17], [18], [19], [20]. In [4], distributed averaging is employed to find a global voltage estimate with which voltage regulation is achieved, but the microgrid dynamics are neglected in the stability analysis. Distributed averaging with dynamic microgrid models is used in [5] and [12] although Tucci et al. [5] require linear matrix inequalities (LMIs) to be solved before buses are allowed to connect and Trip et al. [12] only consider constant current loads. Similarly, a sliding-mode controller is proposed in [13] for a dynamic microgrid with constant current loads. On the other hand, Sadabadi et al. [14] propose a cyberattack-resilient controller for a microgrid with constant conductance loads and resistive lines. A consensus-based distributed controller with event-triggered communication is presented in [15]. Consensus-based controllers are also utilized in [6], [16], and [17], where Zhao and Dörfler [6] use a consensus-based integral layer on top

of a droop-based controller. Finally, while many contributions strive to achieve proportional current sharing [4], [5], [6], [12], [13], [14], [15], [16], [17], [20], nonlinear controllers that achieve proportional power sharing have also been proposed in [18] and [19].

While the literature listed above differs greatly in their approaches, we note a commonality in their omission of buses without actuation. This omission is typically motivated either by considering a microgrid comprising only actuated DGU buses [4], [5], [16], [17], or by eliminating the unactuated buses with the Kron-reduction [6], [12], [13], [14], [15], [18], [19], [20]. However, considering a network comprising only actuated buses severely limits the flexibility of a microgrid since each bus must be able to supply or consume enough power at all times. On the other hand, the Kron-reduction requires loads to be described as positive conductances (see [21]). While research into Kron-reduced networks with negative loads is ongoing (see [22]), the general inclusion of negative loads, e.g., noncontrollable power sources, in Kron-reducible networks remains out of reach at present. Furthermore, consider the case where a DGU can no longer supply or consume the required amount of power, e.g., a fully charged or discharged battery storage. Such a DGU then loses the ability to regulate itself and fully support the grid. In the approaches considered above [4], [5], [6], [12], [13], [14], [15], [16], [17], [18], [19], [20], such a DGU is forced to disconnect from the microgrid and its local measurements are discarded. For DGUs with intermittent power sources, this could result in significant swings in the number of controlled and observed buses in the microgrid.

B. Main Contribution

In this article, we consider a dc microgrid as a physically interconnected multi-agent system. Extending our work in [23], we propose a four-stage controller that achieves voltage regulation and proportional power sharing in a dc microgrid with actuated and unactuated buses in a distributed manner. The four-stage controller comprises a nonlinear weighting function, two dynamic distributed averaging (DDA) stages and a proportional–integral (PI) controller. In detail, the contributions comprise the following:

1) a four-stage distributed controller for dc microgrids that achieves regulation of the weighted average voltage error of actuated and unactuated buses and assures coordination through proportional power sharing at the actuated buses;
2) a nonlinear weighting function that penalizes voltage errors outside a given tolerance band more strongly than those within;
3) passivity classifications for each of the constitutive microgrid subsystems (DGUs, loads, and lines) and for each of the controller stages (weighting function, DDA, and PI);
4) a method for calculating the input-feedforward output-feedback passive (IF-OFP) indices of the nonlinear power-controlled DGUs through optimization.
5) An IF-OFP formulation for the dc microgrid with a supply rate that is independent of the network topology, the number of buses, and their states of actuation;
6) sufficient conditions for the asymptotic stability of the equilibrium manifold of the controlled dc microgrid.

In addition to the contributions listed above, we also contribute a theoretical result comprising a formalization of the obstacle presented by cascaded input-feedforward passive (IFP) and output-feedback passive (OFP) systems in the analysis of dissipative systems. This theoretical contribution informs and motivates parameter choices for the four-stage controller in Contribution 1.

We highlight that the proposed controller can achieve exact voltage regulation and proportional power sharing with the stability verified with the eigenvalues of the linearized system. Moreover, by employing leaky PI controllers and using a passivity-based analysis, we derive sufficient conditions to ensure that the controlled microgrid has an asymptotically stable equilibrium manifold. These conditions, along with the resulting asymptotic stability, are robust against changes in the communication topology, changes in the electrical topology, load changes, changes in the actuation status of DGUs, uncertainties in component parameters, and buses connecting or disconnecting. The main improvement over our work in [23] comprises the flexibility afforded by this topology-independent passivity-based stability analysis[1] along with the addition of a nonlinear weighting function that improves the steady-state characteristics. Additionally, the analytically derived IF-OFP supply rate for the dc microgrid represents an improvement over the numerically derived static network representation in [23].

C. Article's Organization

The introduction concludes with some notation and preliminaries on graph theory. In Section II, we recall and introduce results relating to dissipativity theory. Next, in Section III, the problem is modeled and objectives for the steady state are formalized. In Section IV, a four-stage control structure is introduced that fulfills objectives from Section III. Thereafter, the passivity properties of the constituent subsystems are investigated in Section V and the controller is designed for asymptotic stability of the closed loop in Section VI. Finally, in Section VII, a simulation is used to verify the asymptotic stability and robustness of the closed loop. Concluding remarks are provided in Section VIII.

D. Notation and Preliminaries

Define as a vector $\boldsymbol{a} = (a_k)$ and a matrix $\boldsymbol{A} = (a_{kl})$. The vector $\mathbb{1}_k$ is a k-dimensional vector of ones, and $\boldsymbol{I}_k$ is the identity matrix of dimension k. Diag[$\cdot$] creates a (block-) diagonal matrix from the supplied vectors (or matrices). Let $\boldsymbol{A} \succ 0$ ($\succcurlyeq 0$) denote a positive-(semi)definite matrix. The upper and lower limits of a value a are given by $\overline{a}$ and $\underline{a}$. For a variable x, we denote its unknown steady state as $\hat{x}$, its error

[1] In [23], the stability must be reevaluated whenever topology changes occur.

state as $\tilde{x} \coloneqq x - \hat{x}$, and a desired setpoint as x^*. Whenever clear from context, we omit the time dependence of variables.

We denote by $\mathcal{G} = (\mathcal{N}, \mathcal{E})$ a finite, weighted, undirected graph with vertices $\mathcal{N}$ and edges $\mathcal{E} \subseteq \mathcal{N} \times \mathcal{N}$. Let $|\mathcal{N}|$ be the cardinality of the set $\mathcal{N}$. Let $\boldsymbol{\mathcal{L}}$ be the Laplacian matrix of $\mathcal{G}$. By arbitrarily assigning directions to each edge in $\mathcal{E}$, the incidence matrix $\boldsymbol{E} \in \mathbb{R}^{|\mathcal{N}|\times|\mathcal{E}|}$ of $\mathcal{G}$ is defined by

$$e_{kl} = \begin{cases} +1, & \text{if vertex } k \text{ is the sink of edge } l \\ -1, & \text{if vertex } k \text{ is the source of edge } l \\ 0, & \text{otherwise.} \end{cases} \tag{1}$$

II. Dissipativity Preliminaries

We here recall and introduce preliminaries of dissipativity theory for nonlinear systems. In Section II-A, we provide definitions relating to dissipativity and passivity theory. Thereafter, in Section II-B, we investigate the passivity properties of static functions. Finally, in Section II-C, we recall a result on the interconnection of dissipative systems with quadratic supply rates and formalize a new result on the limitations of such an interconnection.

A. Dissipative Systems

Consider a nonlinear system

$$\begin{cases} \dot{\boldsymbol{x}} = \boldsymbol{f}(\boldsymbol{x}, \boldsymbol{u}) \\ \boldsymbol{y} = \boldsymbol{h}(\boldsymbol{x}) \end{cases} \tag{2}$$

where $\boldsymbol{x} \in \mathbb{R}^n$, $\boldsymbol{u} \in \mathbb{R}^m$, and $\boldsymbol{y} \in \mathbb{R}^m$ and where $\boldsymbol{f}: \mathbb{R}^n \times \mathbb{R}^m \to \mathbb{R}^n$ and $\boldsymbol{h}: \mathbb{R}^n \to \mathbb{R}^m$ are class C^1 functions.

Definition 1 (Dissipative System, See [24], [25], [26]): A system (2) with a class C^1 storage function $S: \mathbb{R}^n \times \mathbb{R}^m \to \mathbb{R}_+$ is dissipative with respect to a supply rate $w(\boldsymbol{u}, \boldsymbol{y})$ if $\dot{S} \leq w(\boldsymbol{u}, \boldsymbol{y})$.

Definition 2 (Quadratic Supply Rates, See [24], [25], [26]): A system (2) that is dissipative with respect to $w(\boldsymbol{u}, \boldsymbol{y})$ is: 1) passive if $w = \boldsymbol{u}^{\mathrm{T}}\boldsymbol{y}$; 2) IFP if $w = \boldsymbol{u}^{\mathrm{T}}\boldsymbol{y} - \nu\boldsymbol{u}^{\mathrm{T}}\boldsymbol{u}$; 3) OFP if $w = \boldsymbol{u}^{\mathrm{T}}\boldsymbol{y} - \rho\boldsymbol{y}^{\mathrm{T}}\boldsymbol{y}$; 4) IF-OFP if $w = (1 + \nu\rho)\boldsymbol{u}^{\mathrm{T}}\boldsymbol{y} - \nu\boldsymbol{u}^{\mathrm{T}}\boldsymbol{u} - \rho\boldsymbol{y}^{\mathrm{T}}\boldsymbol{y}$; and 5) has an L_2-gain of γ_{L_2} if $w = \gamma_{L_2}^2\boldsymbol{u}^{\mathrm{T}}\boldsymbol{u} - \boldsymbol{y}^{\mathrm{T}}\boldsymbol{y}$, where $\gamma_{L_2} > 0$ and $\nu, \rho \in \mathbb{R}$.

Definition 3 (Zero-State Observable (ZSO) [24, p. 46]): A system (2) is ZSO if $\boldsymbol{u} \equiv \boldsymbol{0}$ and $\boldsymbol{y} \equiv \boldsymbol{0}$ implies $\boldsymbol{x} \equiv \boldsymbol{0}$.

For cases where the desired equilibrium of a system is not at the origin but at some constant value, the shifted passivity [24, p. 96] or equilibrium-independent passivity (EIP) [27] of a system must be investigated. Naturally, this requires that an equilibrium exists, i.e., there is a unique input $\hat{\boldsymbol{u}} \in \mathbb{R}^m$ for every equilibrium $\hat{\boldsymbol{x}} \in \hat{\mathcal{X}} \subset \mathbb{R}^n$ such that (2) produces $\boldsymbol{f}(\hat{\boldsymbol{x}}, \hat{\boldsymbol{u}}) = \boldsymbol{0}$ and $\hat{\boldsymbol{y}} = \boldsymbol{h}(\hat{\boldsymbol{x}}, \hat{\boldsymbol{u}})$ [28, p. 24].

Definition 4 (EIP [28, p. 24]): A system (2) is EIP if there exists a class C^1 storage function $S(\boldsymbol{x}, \hat{\boldsymbol{x}})$, $S: \mathbb{R}^n \times \hat{\mathcal{X}} \to \mathbb{R}_+$, with $S(\hat{\boldsymbol{x}}, \hat{\boldsymbol{x}}) = 0$, that is dissipative with respect to $w(\boldsymbol{u} - \hat{\boldsymbol{u}}, \boldsymbol{y} - \hat{\boldsymbol{y}})$ for any equilibrium $(\hat{\boldsymbol{u}}, \hat{\boldsymbol{y}})$.

B. Passive Static Functions

Recall that a sector-bounded static nonlinear function is dissipative to a supply rate defined by the sector bound [26, Def. 6.2]. We now consider the arbitrarily shifted single-input single-output function

$$\begin{cases} y = h(u), \quad u, \hat{u} \in \mathcal{U}, \ y, \hat{y} \in \mathcal{Y}, \ h: \mathcal{U} \to \mathcal{Y} \\ \tilde{y} = \tilde{h}(\tilde{u}) \coloneqq h(u) - h(\hat{u}) = y - \hat{y}, \quad \tilde{u} \coloneqq u - \hat{u} \end{cases} \tag{3}$$

and show how its dissipativity properties may be derived.

Proposition 5 (EIP Static Functions): A static function (3) of class C^0 is IF-OFP($\underline{c}$, $1/\overline{c}$) with respect to the arbitrarily shifted input–output pair $(\tilde{u}, \tilde{y})$ if

$$\underline{c} \leq \frac{dh(u)}{du} \leq \overline{c} \quad \forall u \in \mathcal{U} \tag{4}$$

and $0 < \overline{c} < \infty$.

Proof: Consider, for (3), the slope between an arbitrary shift $(\hat{u}, \hat{y}) \in \mathcal{U} \times \mathcal{Y}$ and a point (u, y), for which the upper and lower bounds are given by

$$\underline{c} \leq \frac{y - \hat{y}}{u - \hat{u}} \leq \overline{c} \quad \forall (u, y), (\hat{u}, \hat{y}) \in \mathcal{U} \times \mathcal{Y}. \tag{5}$$

Changing (5) to the shifted variables $\tilde{u}$ and $\tilde{y}$ and multiplying through by $\tilde{u}^2$ yields

$$\begin{aligned} \underline{c}\tilde{u}^2 \leq \tilde{u}\tilde{y} \leq \overline{c}\tilde{u}^2 \iff (\tilde{y} - \underline{c}\tilde{u})(\tilde{y} - \overline{c}\tilde{u}) \leq 0 \\ \iff (\tilde{y} - \underline{c}\tilde{u})(1/\overline{c}\,\tilde{y} - \tilde{u}) \leq 0 \end{aligned} \tag{6}$$

for $\overline{c} > 0$, which describes an IF-OFP function (see [26, p. 231]). Finally, through the mean value theorem, the bounds in (5) may be found from (4). ∎

We note that the restrictions on $\overline{c}$ in Proposition 5 are needed from a computational point of view ($\overline{c} < \infty$) and to ensure that the passivity indices correspond to the correct sector[2] ($\overline{c} > 0$). However, this limits the passivity properties attainable through Proposition 5 to $\rho = 1/\overline{c} > 0$.

Remark 1 (Symmetrical Sectors): Placing the additional restriction $\underline{c} = -\overline{c}$ in (4) results in the Lipschitz continuity of $h(u)$. Moreover, this implies that the arbitrarily shifted function $\tilde{h}(\tilde{u})$ has a finite L_2-gain of $\overline{c}$ (see [28, p. 24], [29, Lemma 4]).

C. Interconnected Quadratic Dissipative Systems

Building upon the results on the interconnection of dissipative systems in [28] and [30], we now provide a method for finding dissipativity properties for a subset of the interconnected subsystems such that interconnected stability is guaranteed. Specifically, we look for the dissipative supply rates that restrict the subset of subsystems as little as possible. For a set $\mathcal{S}$ of subsystems, define $\boldsymbol{u} = [\boldsymbol{u}_1^{\mathrm{T}}, \ldots, \boldsymbol{u}_{|\mathcal{S}|}^{\mathrm{T}}]^{\mathrm{T}}$ and $\boldsymbol{y} = [\boldsymbol{y}_1^{\mathrm{T}}, \ldots, \boldsymbol{y}_{|\mathcal{S}|}^{\mathrm{T}}]^{\mathrm{T}}$.

Theorem 6 (Minimally Restrictive Stabilizing Indices): Consider $|\mathcal{S}|$ subsystems of the form (2) that are dissipative with respect to the supply rates $w_i = 2\sigma_i\boldsymbol{u}_i^{\mathrm{T}}\boldsymbol{y}_i - \nu_i\boldsymbol{u}_i^{\mathrm{T}}\boldsymbol{u}_i - \rho_i\boldsymbol{y}_i^{\mathrm{T}}\boldsymbol{y}_i$ and are linearly interconnected according to $\boldsymbol{u} = \boldsymbol{H}\boldsymbol{y}$. The stability of the interconnected system is guaranteed if

[2]Consider, e.g., the sector Proposition 5 would yield if $\underline{c} \leq \overline{c} < 0$.

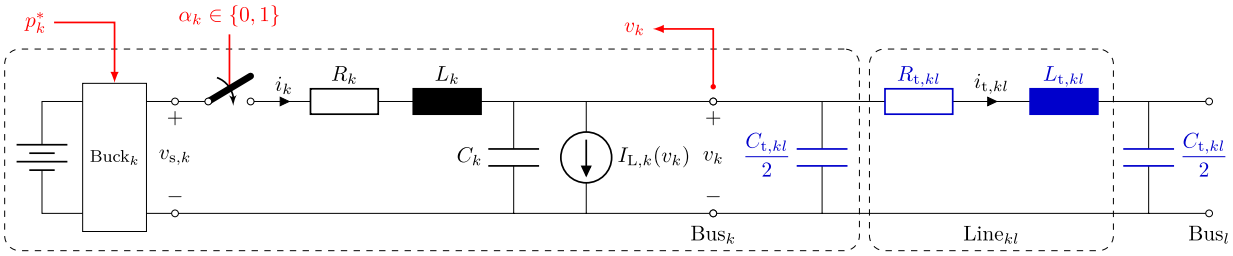

Fig. 1. Circuit diagram of a bus comprising a dc–dc buck converter, a filter, and a current source representing a load, connected to a π-model line (blue); the line capacitances are considered to be part of the respective buses.

there exists a $\boldsymbol{D}$ and $\nu_j, \rho_j \in \mathbb{R}$ with $j \in \mathcal{J}$ such that a solution to the optimization problem

$$\begin{aligned} \min_{\boldsymbol{D},\, \substack{\nu_j,\, \rho_j,\\ j\in\mathcal{J}}} & \sum_{j\in\mathcal{J}} (\nu_j + \rho_j) \\ \text{s.t. } & \sigma_j = 1/2(1+\nu_j\rho_j), \quad j \in \mathcal{J} \\ & \boldsymbol{Q} \prec 0, \quad \boldsymbol{D}^2 \succ 0 \end{aligned} \tag{7}$$

exists, where the subsystems with configurable supply rates are represented by the set $\mathcal{J} \subset \mathcal{S}$, and

$$\boldsymbol{Q} \coloneqq \begin{bmatrix} \boldsymbol{H} \\ \boldsymbol{I} \end{bmatrix}^{\mathrm{T}} \boldsymbol{D}\boldsymbol{W}\boldsymbol{D} \begin{bmatrix} \boldsymbol{H} \\ \boldsymbol{I} \end{bmatrix} \tag{8}$$

$$\boldsymbol{D} \coloneqq \operatorname{Diag}[\boldsymbol{d}^{\mathrm{T}}, \boldsymbol{d}^{\mathrm{T}}], \quad \boldsymbol{d} = (\sqrt{d_i}) \tag{9}$$

$$\boldsymbol{W} \coloneqq \begin{bmatrix} -\operatorname{Diag}[\nu_i] & \operatorname{Diag}[\sigma_i] \\ \operatorname{Diag}[\sigma_i] & -\operatorname{Diag}[\rho_i] \end{bmatrix}, \quad i \in \mathcal{S}. \tag{10}$$

The proof for Theorem 6 follows analogously to the proof of [29, Theorem 13] with the application of [29, Remark 5] and thus is omitted for brevity. Note that if $\mathcal{J} = \emptyset$ in (7), Theorem 6 can be used to verify the stability of interconnected dissipative systems.

Despite the design flexibility provided by Theorem 6, certain cascade configurations present obstacles to the application of dissipativity theory. The following proposition formalizes the problem presented by one such configuration, which arises in the sequel and is used to inform the control design.

Proposition 7 (Nondissipativity of Cascaded IFP–OFP Systems): Consider $|\mathcal{S}| \geq 2$ subsystems (2) which are dissipative with respect to $w_i = 2\sigma_i \boldsymbol{u}_i^{\mathrm{T}}\boldsymbol{y}_i - \nu_i \boldsymbol{u}_i^{\mathrm{T}}\boldsymbol{u}_i - \rho_i \boldsymbol{y}_i^{\mathrm{T}}\boldsymbol{y}_i$ and linearly interconnected according to $\boldsymbol{u} = \boldsymbol{H}\boldsymbol{y}$. Let $i = 1$ and $i = 2$ arbitrarily denote subsystems that are IFP and OFP, respectively. If these systems are connected in exclusive cascade and do not form a feedback connection, i.e.,

$$\boldsymbol{H} = \begin{bmatrix} 0 & 0 & * \\ 1 & 0 & \boldsymbol{0} \\ \boldsymbol{0} & * & * \end{bmatrix} \tag{11}$$

then investigating stability via separable storage functions as in Theorem 6 fails.

Proof: Evaluating the stability criteria in (7) under the imposed IFP and OFP conditions yields the $\boldsymbol{Q}$ (8) entries

$$q_{11} = d_1\rho_1 + d_2\nu_2 = 0, \quad q_{12} = q_{21} = \frac{d_2\sigma_2}{2} = \frac{d_2}{2}. \tag{12}$$

Since $d_i > 0$, $\boldsymbol{Q}$ constitutes an indefinite saddle point matrix [31, Section 3.4], violating the requirement in (7). ■

Remark 2 (Nonseparable Storage Functions): The obstacle in Proposition 7 arises due to the storage functions being compartmentalized by the subsystem boundaries. While the separability of storage functions is a central motivation for the use of dissipativity theory, forgoing this allows for a stability analysis through less conservative methods (e.g., the Kalman–Yakubovich–Popov (KYP) lemma).

III. Problem Description

In this section, the components comprising the dc microgrid are introduced in Section III-A. This is followed by Section III-B, where controllers are added that regulate the output power of actuated buses in order to facilitate power sharing in the sequel. Finally, we formulate the coordination and cooperation goals as a control problem in Section III-C.

A. DC Network

We consider a dc microgrid comprising $N = |\mathcal{N}|$ buses connected by via π-model electrical lines, as depicted in Fig. 1. Let the graph $\mathcal{G}_{\mathrm{P}} = (\mathcal{N}, \mathcal{E}_{\mathrm{P}})$ describe the interconnection with $\mathcal{N}$ as the set of buses and $\mathcal{E}_{\mathrm{P}}$ as the set of lines. Without loss of generalization, we allow each node to inject power through a dc–dc buck converter connected via a lossy LC-filter. Note that a time-averaged model (see [9], [10], [12]) is used for the buck converter and the energy source is assumed to be ideal but finite.

Let the buses be split into an actuated set $\mathcal{N}_\alpha$ and an unactuated set $\mathcal{N}_\beta$, according to whether the buck converter can freely regulate the amount of power injected at a given time. Buses may freely switch between the sets $\mathcal{N}_\alpha$ and $\mathcal{N}_\beta$, but $\mathcal{N}_\alpha \cap \mathcal{N}_\beta = \emptyset$ and $\mathcal{N}_\alpha \cup \mathcal{N}_\beta = \mathcal{N}$ always hold. To characterize this actuation state of a bus, define the piecewise-constant, time-varying actuation parameter $\alpha_k(t)$ as

$$\alpha_k(t) \coloneqq \begin{cases} 1, & k \in \mathcal{N}_\alpha \\ 0, & k \in \mathcal{N}_\beta. \end{cases} \tag{13}$$

Note that we omit the time dependence of α_k in the sequel.

The dynamics for actuated buses with DGUs, where $\alpha_k = 1$ with $k \in \mathcal{N}_\alpha$, are described by (see [9], [10], [12])

$$\begin{bmatrix} L_k\dot{i}_k \\ C_{\mathrm{eq},k}\dot{v}_k \end{bmatrix} = \begin{bmatrix} -R_k & -1 \\ 1 & 0 \end{bmatrix} \begin{bmatrix} i_k \\ v_k \end{bmatrix} + \begin{bmatrix} v_{s,k} \\ -\boldsymbol{e}_{\mathrm{P,r},k}^{\mathrm{T}}\boldsymbol{i}_{\mathrm{t}} - I_{\mathrm{L},k}(v_k) \end{bmatrix} \tag{14}$$

where $C_{\mathrm{eq},k} = C_k + (1/2)\boldsymbol{e}_{\mathrm{P,r},k}^{\mathrm{T}} \operatorname{Diag}[\boldsymbol{C}_{\mathrm{t}}]\boldsymbol{e}_{\mathrm{P,r},k}$; $C_k, L_k > 0$; $i_k \in \mathbb{R}$; $v_k \in \mathbb{R}_+$; and $\boldsymbol{C}_{\mathrm{t}} = (C_{kl})$ is the vector of the line capacitances, with $C_{kl} > 0$ for each $kl \in \mathcal{E}_{\mathrm{P}}$. The line currents $\boldsymbol{i}_{\mathrm{t}}$ connect to the capacitor voltages according to incidence matrix $\boldsymbol{E}_{\mathrm{P}}^{\mathrm{T}} = (\boldsymbol{e}_{\mathrm{P,r},k}^{\mathrm{T}})$ of $\mathcal{G}_{\mathrm{P}}$.[3] The dynamics of the unactuated

[3] $\boldsymbol{e}_{\mathrm{P,r},k}^{\mathrm{T}}$ selects the row from $\boldsymbol{E}_{\mathrm{P}}$ corresponding to bus k.

load buses with $\alpha_k = 0$ correspond to the simplified system

$$C_{\mathrm{eq},k}\dot{v}_k = -\boldsymbol{e}_{\mathrm{P,r},k}^{\mathrm{T}}\boldsymbol{i}_{\mathrm{t}} - I_{\mathrm{L},k}(v_k), \quad k \in \mathcal{N}_\beta. \tag{15}$$

In both the actuated (14) and unactuated (15) cases, the loads are considered static, nonlinear voltage-dependent current sources, which are described by class C^0 functions. In this work, we utilize the standard impedance, current, and power (ZIP)-model comprising constant impedance, constant current, and constant power parts. Note that other continuous functions may also be used without restriction.[4] As described in [33, pp. 110–112], we define a critical voltage v_{crit}, typically set to $0.7v_{\mathrm{Ref}}$, below which the loads are purely resistive. Thus,

$$I_{\mathrm{L},k}(v_k) = \begin{cases} Z_k^{-1}v_k + I_k + \dfrac{P_k}{v_k}, & v_k \geq v_{\mathrm{crit}} \\ Z_{\mathrm{crit},k}^{-1}v_k, & v_k < v_{\mathrm{crit}} \end{cases} \tag{16}$$

$$Z_{\mathrm{crit},k}^{-1} := \frac{I_{\mathrm{L},k}(v_{\mathrm{crit}})}{v_{\mathrm{crit}}} = Z_k^{-1} + \frac{I_k}{v_{\mathrm{crit}}} + \frac{P_k}{v_{\mathrm{crit}}^2} \tag{17}$$

describe a static, nonlinear load that conforms to (3).

Lastly, the π-model transmission lines physically connecting the nodes are governed by the dynamics

$$L_{\mathrm{t},kl}\dot{i}_{\mathrm{t},kl} = -R_{\mathrm{t},kl}i_{\mathrm{t},kl} + \boldsymbol{e}_{\mathrm{P,c},kl}^{\mathrm{T}}\boldsymbol{v}, \quad kl \in \mathcal{E}_{\mathrm{P}} \tag{18}$$

where $i_{\mathrm{t},kl} \in \mathbb{R}$, $L_{\mathrm{t},kl}, R_{\mathrm{t},kl} > 0$, and $(\boldsymbol{e}_{\mathrm{P,c},kl}) = \boldsymbol{E}_{\mathrm{P}}$.[5] Note that the line capacitances are included in the equivalent capacitances $C_{\mathrm{eq},k}$ at the buses.

B. DGU Power Regulator

To allow for power sharing between the actuated buses (14) in the sequel, we equip each DGU with a controller that can regulate the injected power to a desired power setpoint p_k^*. This regulator has the form

$$\begin{aligned} \dot{e}_{\mathrm{d},k} &= \alpha_k\left(p_k^* - p_k\right) \\ v_{\mathrm{s},k} &= k_{\mathrm{d}}^P\left(p_k^* - p_k\right) + k_{\mathrm{d}}^I e_{\mathrm{d},k} + \tilde{R}i_k + v_{\mathrm{Ref}} \end{aligned} \tag{19}$$

where $e_{\mathrm{d}} \in \mathbb{R}$, $p_k = v_k i_k$ is the actual power injected, $\tilde{R} \in \mathbb{R}$ is the damping added to the system, and $k_{\mathrm{d}}^P, k_{\mathrm{d}}^I > 0$ are the control parameters. Since the DGU power ratings may differ, we define the normalized power setpoint ϕ_k^* as

$$\eta_k\phi_k^* := p_k^* \tag{20}$$

where $\eta_k \in [\underline{\eta}; \overline{\eta}] \subset \mathbb{R}_+$ is a constant dimensionless gain with a lower bound $\underline{\eta} > 0$. Combining (19) and (20) with (14) yields the nonlinear system for the actuated agents

$$\begin{bmatrix} \dot{e}_{\mathrm{d},k} \\ L_k\dot{i}_k \\ C_{\mathrm{eq},k}\dot{v}_k \end{bmatrix} = \begin{bmatrix} 0 & -v_k & 0 \\ k_{\mathrm{d}}^I & \tilde{R} - R_k - k_{\mathrm{d}}^P v_k & -1 \\ 0 & 1 & 0 \end{bmatrix} \begin{bmatrix} e_{\mathrm{d},k} \\ i_k \\ v_k \end{bmatrix} + \begin{bmatrix} \eta_k\phi_k^* \\ k_{\mathrm{d}}^P\eta_k\phi_k^* + v_{\mathrm{Ref}} \\ -\boldsymbol{e}_{\mathrm{P,r},k}^{\mathrm{T}}\boldsymbol{i}_{\mathrm{t}} - I_{\mathrm{L},k}(v_k) \end{bmatrix}, \quad k \in \mathcal{N}_\alpha. \tag{21}$$

Remark 3 (Regulating Current or Voltage): Without invalidating the stability analysis in the sequel, the regulator in (19) can be exchanged for simpler, purely linear current or voltage regulators (see [9], [10], [11]).

Remark 4 (Constrained DGU Operation): If an actuated DGU cannot provide the desired power p_k^*, e.g., due to current, storage, or temperature limitations, the DGU may simply set its actuation state $\alpha_k = 0$ to disable its control.

C. Control Problem

A central requirement for dc microgrids is voltage stability, which requires the bus voltages to remain within a given tolerance band around the reference v_{Ref}. Specifically, this requirement should be met throughout the network, and not only at the actuated buses. Due to the presence of lossy lines, power flows are associated with voltage differences between buses, meaning that $v_k \to v_{\mathrm{Ref}}, \forall k \in \mathcal{N}$ is not practical. Ideally, the voltages at all buses should be arrayed in a tolerance band around v_{Ref} and be as close to v_{Ref} as possible.[6] The manipulated variables used to achieve this are the normalized power setpoints ϕ_k^* supplied to the actuated DGUs (19). This leads to the first objective for the control of the dc microgrid, which involves finding the setpoints ϕ_k^* that ensure the weighted average voltage equals v_{Ref} at steady state.

Objective 1 (Weighted Voltage Consensus):

$$\text{Find } \phi_k^*, \quad \text{s.t. } \lim_{t\to\infty}\frac{1}{N}\sum_{k\in\mathcal{N}} h(v_k(t)) = v_{\mathrm{Ref}} \tag{22}$$

for a strictly increasing weighting function $h : \mathbb{R} \to \mathbb{R}$.

By choosing a nonlinear h, large voltage errors may be weighed more strongly. This allows for better utilization of the tolerance band since bus voltages can be further from v_{Ref} before registering as a significant error.

In addition to Objective 1, proportional power sharing is typically desired so that the loads are not supplied only by small subset of the actuated DGUs. By spreading out the injection of power across all actuated DGUs, the DGUs are stressed equally, which reduces the likelihood of stress-related hardware failures. We, thus, formulate the second objective as requiring uniform setpoints for the DGUs in steady state.

Objective 2 (Cooperative Proportional Power Sharing):

$$\lim_{t\to\infty}\left(\phi_k^*(t) - \phi_l^*(t)\right) = 0 \quad \forall k, l \in \mathcal{N}. \tag{23}$$

Achieving Objectives 1 and 2, thus, yields a controlled microgrid where the average weighted voltage error of all buses tends to zero through the coordinated proportional action of the actuated buses in a distributed fashion. These objectives also allow DGUs to transition seamlessly between actuated and unactuated states and ensure no measurement information is discarded because a bus is not regulated. Notice that disregarding the unactuated buses in Objectives 1 and 2 yields the objectives typically used in the literature [4], [6], [12], [13], [14], [16], [17], [20].

To achieve these objectives, we make the following assumptions related to appropriate network design.

Assumption 1 (Feasible Network): The available power sources can feasibly supply the loads with power over the given electrical network, i.e., a suitable equilibrium for the microgrid exists.

[4]This includes exponential loads (see [32]).

[5]$\boldsymbol{e}_{\mathrm{P,c},kl}$ selects the column from $\boldsymbol{E}_{\mathrm{P}}$ corresponding to line kl.

[6]The magnitude of the errors $v_{\mathrm{Ref}} - v_k$ strongly depend on the loads and line resistance. Therefore, small errors presuppose adequate network design.

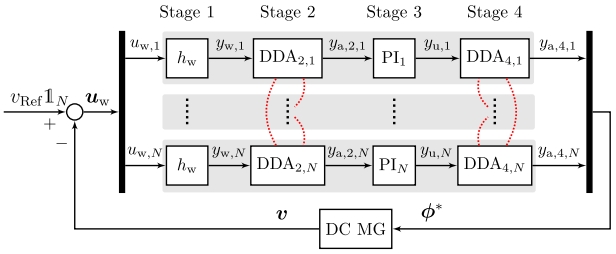

Fig. 2. Distributed four-stage control connected in feedback to the microgrid and with indicated communication links ⋯ between the local control structures.

Assumption 2 (Number of Actuated DGUs): At least one DGU is actuated at any given time, i.e., $\mathcal{N}_\alpha \neq \emptyset$.

Assumption 3 (Connected Topologies): Objectives 1 and 2 only apply to a subset of buses electrically connected as per $\mathcal{G}_{\mathrm{P}}$. Moreover, for a distributed control, a connected communication graph exclusively interconnects the same subset of buses.

Note that Assumption 1 is typically made implicitly or explicitly in the literature (see the discussion in [16]). Assumptions 2 and 3 further specify requirements that allow a distributed control to achieve the feasible state in Assumption 1, i.e., by ensuring that at least one source of stabilization is present in the network (Assumption 2) and by ensuring that the coordination corresponds to the network to be controlled (Assumption 3).

IV. Control Structure

To meet Objectives 1 and 2, we propose the four-stage control structure depicted in Fig. 2. This control structure comprises two DDA implementations separated by agent PI controllers local to the buses as in [23]. This is prepended by a nonlinear weighting function h_{w}. In Sections IV-A–IV-C, we successively introduce these respective subsystems. Finally, in Section IV-D, we show that the control structure meets the objectives.

A. DDA Controller

Consider the communication graph $\mathcal{G}_{\mathrm{C}} = (\mathcal{N}, \mathcal{E}_{\mathrm{C}})$ linking the buses of the dc microgrid. The communication graph comprises the same vertices as the physical interconnection graph $\mathcal{G}_{\mathrm{P}}$ but possibly with a different topology. Let $\boldsymbol{\mathcal{L}}_{\mathrm{C}}$ denote the Laplacian of $\mathcal{G}_{\mathrm{C}}$. For Stages 2 and 4 of the control structure, each agent implements an instance of the DDA[7] described in [34]. The instances of the respective stages may be combined into the vector form as

$$\mathrm{DDA}_s \begin{cases} \begin{bmatrix} \dot{\boldsymbol{x}}_{\mathrm{a},s} \\ \dot{\boldsymbol{z}}_{\mathrm{a},s} \end{bmatrix} = \begin{bmatrix} -\gamma_{\mathrm{a}}\boldsymbol{I}_N - \boldsymbol{\mathcal{L}}_{\mathrm{C},P} & \boldsymbol{\mathcal{L}}_{\mathrm{C},I}^{\mathrm{T}} \\ -\boldsymbol{\mathcal{L}}_{\mathrm{C},I} & \boldsymbol{0} \end{bmatrix} \begin{bmatrix} \boldsymbol{x}_{\mathrm{a},s} \\ \boldsymbol{z}_{\mathrm{a},s} \end{bmatrix} \\ \qquad\qquad + \begin{bmatrix} \gamma_{\mathrm{a}}\boldsymbol{I}_N \\ \boldsymbol{0} \end{bmatrix} \boldsymbol{u}_{\mathrm{a},s} \\ \boldsymbol{y}_{\mathrm{a},s} = \boldsymbol{x}_{\mathrm{a},s} \end{cases} \tag{24}$$

where $s \in \{2, 4\}$ denotes the stage in Fig. 2, and $\boldsymbol{x}_{\mathrm{a},s}, \boldsymbol{z}_{\mathrm{a},s} \in \mathbb{R}^N$ are the consensus and integral states, respectively. Furthermore, $\gamma_{\mathrm{a}} > 0$ is a global estimator parameter (see [34]), and $\boldsymbol{\mathcal{L}}_{\mathrm{C},I} = k_{\mathrm{a}}^I \boldsymbol{\mathcal{L}}_{\mathrm{C}}$ and $\boldsymbol{\mathcal{L}}_{\mathrm{C},P} = k_{\mathrm{a}}^P \boldsymbol{\mathcal{L}}_{\mathrm{C}}$ are the Laplacian matrices weighted for the integral and proportional responses, respectively. Recall from [34] that a constant input $\boldsymbol{u}_{\mathrm{a},s}$ yields

$$\lim_{t\to\infty} y_{\mathrm{a},s,k} = \frac{\boldsymbol{u}_{\mathrm{a},s}^{\mathrm{T}}\mathbb{1}_N}{N} \quad \forall k. \tag{25}$$

[7]We implement the PI-DDA variant proposed in [34] and use the same communication graph for the proportional and integral terms.

B. Agent PI Controller

In Stage 3, we equip each bus $k \in \mathcal{N}$ with a leaky agent PI controller similar to the approach in [35]

$$\mathrm{PI}_k \begin{cases} \dot{x}_{\mathrm{u},k} = -\zeta_{\mathrm{u}} x_{\mathrm{u},k} + u_{\mathrm{u},k} \\ y_{\mathrm{u},k} = k_{\mathrm{u}}^I x_{\mathrm{u},k} + k_{\mathrm{u}}^P u_{\mathrm{u},k} \end{cases} \tag{26}$$

where $x_{\mathrm{u},k} \in \mathbb{R}$, $\zeta_{\mathrm{u}} \geq 0$, and $k_{\mathrm{u}}^P, k_{\mathrm{u}}^I > 0$. Note that $\zeta_{\mathrm{u}} = 0$ reduces (26) to an ideal PI controller. The combined form of the N agent controllers is

$$\begin{aligned} \dot{\boldsymbol{x}}_{\mathrm{u}} &= -\zeta_{\mathrm{u}}\boldsymbol{x}_{\mathrm{u}} + \boldsymbol{u}_{\mathrm{u}} \\ \boldsymbol{y}_{\mathrm{u}} &= k_{\mathrm{u}}^I \boldsymbol{x}_{\mathrm{u}} + k_{\mathrm{u}}^P \boldsymbol{u}_{\mathrm{u}}. \end{aligned} \tag{27}$$

Remark 5 (Nonideal Integrators): As shown in the sequel, ideal PI controllers only exhibit an IFP property, whereas the DDA controller is OFP. The interconnection in Fig. 2, thus, yields a cascaded IFP–OFP structure that obstructs the dissipativity analysis (see Proposition 7). The use of leaky integrators ($\zeta_{\mathrm{u}} > 0$) overcomes this obstacle at the cost of negatively affecting the steady-state properties since (26) forces the equilibrium

$$\boldsymbol{u}_{\mathrm{u}} = \zeta_{\mathrm{u}}\boldsymbol{x}_{\mathrm{u}} \tag{28}$$

instead of $\boldsymbol{u}_{\mathrm{u}} = \boldsymbol{0}$. In the context of Fig. 2, this corresponds to an unwanted steady-state offset for the average weighted voltage error.

Remark 6 (Agent PI Controller Antiwindup): To prevent controller windup, the input to the PI control in (26) should be zeroed for any unactuated agents that are disconnected from the communication network.

Remark 7 (Nonparticipating Agents): Implementing (26) at each bus $k \in \mathcal{N}$ allows for a faster reaction to disturbances at the cost of controller redundancy. By setting $u_{\mathrm{a},4,m} \coloneqq y_{\mathrm{a},4,m}$ at the Stage-4 DDA of the control structure for some agents $m \in \mathcal{M} \subset \mathcal{N}$, the PI control (26) can be omitted at the agents in $\mathcal{M}$ without affecting the steady state. Nevertheless, the measurements of the buses in $k \in \mathcal{M}$ are still included in the Stage-2 DDA. Note that at least one participating agent PI controller is required (see [23, Remark 8]).

C. Weighting Function

To allow for a better utilization of the tolerance band around v_{Ref}, we desire a weighting function that assigns a low gain for errors within the tolerance band and a high gain for larger errors. We, therefore, define the class C^1 function $y_{\mathrm{w},k} = h_{\mathrm{w}}(u_{\mathrm{w},k})$ conforming to (3), where

$$h_{\mathrm{w}}(u) \coloneqq a_{\mathrm{w}}u + b_{\mathrm{w}}g_{\mathrm{w}}(u) - b_{\mathrm{w}}\tanh(g_{\mathrm{w}}(u)) \tag{29}$$

$$g_{\mathrm{w}}(u) \coloneqq \begin{cases} u + c_{\mathrm{w}}, & u < -c_{\mathrm{w}} \\ 0, & -c_{\mathrm{w}} \leq u \leq c_{\mathrm{w}} \\ u - c_{\mathrm{w}}, & c_{\mathrm{w}} < u \end{cases} \tag{30}$$

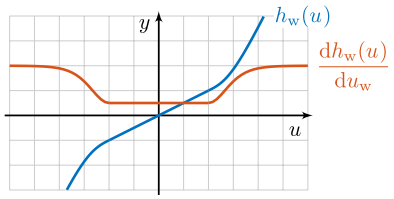

Fig. 3. Example of the weighting function h_w (29) and its derivative (60) on a unit grid, with $a_\mathrm{w} = 0.5$, $b_\mathrm{w} = 1.5$, and $c_\mathrm{w} = 2$.

and where (30) describes a dead-zone parametrized by c_w. An example of (29) is depicted in Fig. 3 along with its derivative. For a strictly increasing function as per Objective 1, set $a_\mathrm{w} > 0$ and $b_\mathrm{w} > -a_\mathrm{w}$.

D. Equilibrium Analysis

In a first step toward analyzing the closed loop, we analyze the assumed equilibrium of the interconnected microgrid and four-stage controller (see Assumption 1). Specifically, we verify that the proposed control yields an equilibrium that satisfies Objectives 1 and 2.

Proposition 8 (Controller Equilibrium Analysis): Consider the dc microgrid comprising (15), (18), and (21) which is connected in feedback with the four-stage controller comprising (24), (27), and (29) as in Fig. 2. Let Assumptions 1, 2, and 3 hold. Then, Objective 2 is met for the equilibrium imposed by the control structure. Moreover, Objective 1 is achieved exactly for ideal integrators $\zeta_\mathrm{u} = 0$ in (27). For lossy integrators with $\zeta_\mathrm{u} > 0$, the remaining error for Objective 1 is be described by the steady-state value of $\boldsymbol{y}_{\mathrm{a},2}$, where

$$\boldsymbol{y}_{\mathrm{a},2} = \frac{\zeta_\mathrm{u}}{k_\mathrm{u}^I \left(1 + \zeta_\mathrm{u} k_\mathrm{u}^P\right)} \boldsymbol{y}_{\mathrm{a},4}. \tag{31}$$

The proof of Proposition 8 can be found in Appendix A. Through Proposition 8, we, thus, confirm that the proposed controller yields an equilibrium which meets the requirements even though the requirements are not perfectly met when leaky agent PI controllers are used. We also note that Proposition 8 only considers the controlled microgrid already in equilibrium and does not consider the convergence to the equilibrium.

Remark 8 (Compensating Leaky Integral Errors): As indicated by (31) in Proposition 8, the leaky agent PI controllers result in a constant steady-state error for the average voltage regulation (Objective 1). Since a positive $\boldsymbol{y}_{\mathrm{a},2}$ corresponds to voltages below the desired v_Ref, it follows that setting v_Ref above the actual desired voltage reference will result in higher bus voltages. Changing v_Ref, thus, allows the steady-state effects of the leaky integrators to be compensated. Moreover, notice that $\boldsymbol{y}_{\mathrm{a},4}$ is the controller output, i.e., the normalized setpoint $\boldsymbol{\phi}^*$ used for the DGUs (see Fig. 2). Thus, the error measure in (31), which is only dependent on the controller output, can be used to determine the offset to v_Ref for exact voltage regulation. Note, however, that modifying v_Ref based on $\boldsymbol{\phi}^*$ results in a new loop, which requires an additional stability analysis.

V. Subsystem Passivity Analysis

Having verified whether the desirable steady state is achieved by the controller, we now set about analyzing the convergence to this steady state. With the aim of applying Theorem 6 for the closed-loop stability, we first analyze the passivity properties of the individual subsystems. Since the steady-state bus voltages $\hat{v}_k$ are unknown and nonzero, we investigate the passivity properties shifted to any plausible point of operation using EIP. To this end, we construct an EIP formulation for the dc microgrid from its constitutive elements in Section V-A. This is followed by the respective analyses of the various controller stages in Section V-B. Note that we omit the bus indices k and l in this section where clear from context.

A. DC Microgrid Passivity

For the stability of the microgrid at the equilibrium $\hat{\boldsymbol{v}}$, we desire an EIP property relating the shifted input setpoints $\tilde{\boldsymbol{\phi}}^* = \boldsymbol{\phi}^* - \hat{\boldsymbol{\phi}}^*$ to the output voltage errors $\tilde{\boldsymbol{v}} = \boldsymbol{v} - \hat{\boldsymbol{v}}$ of all nodes since this port $(\tilde{\boldsymbol{\phi}}^*, \tilde{\boldsymbol{v}})$ is used by the controller in Fig. 2. To this end, we derive EIP properties for the load, DGU, and line subsystems of the microgrid, making sure to shift the subsystem dynamics to the assumed equilibrium in each case (see Assumption 1). Thereafter, we combine the results of these subsystems to construct an EIP property for the microgrid as a whole. Where applicable, an analysis of the zero-state dynamics is performed to ensure the eventual stability of the controlled microgrid.

1) Load Passivity: Let the unactuated bus dynamics in (15) for the buses in $\mathcal{N}_\beta$ be shifted to the equilibrium $(\hat{\boldsymbol{i}}_\mathrm{t}, \hat{v})$, yielding

$$C_\mathrm{eq} \dot{\tilde{v}} = -\boldsymbol{e}_{\mathrm{P,r}}^\mathrm{T} \tilde{\boldsymbol{i}}_\mathrm{t} - \tilde{I}_\mathrm{L}(\tilde{v}) - \left(\boldsymbol{e}_{\mathrm{P,r}}^\mathrm{T} \hat{\boldsymbol{i}}_\mathrm{t} + I_\mathrm{L}(\hat{v})\right) \tag{32}$$

for the static load function shifted according to (3). In (32), $\boldsymbol{e}_{\mathrm{P,r}}^\mathrm{T} \hat{\boldsymbol{i}}_\mathrm{t} = -I_\mathrm{L}(\hat{v})$ since the load is fully supplied by the cumulative line currents in steady state.

Proposition 9 (Load EIP): The shifted load dynamics in (32) are OFP(ρ_L) with respect to the input–output pair $(-\boldsymbol{e}_{\mathrm{P,r}}^\mathrm{T} \tilde{\boldsymbol{i}}_\mathrm{t}, \tilde{v})$ with $\rho_\mathrm{L} = \underline{c}_\mathrm{L}$ the smallest gradient of the static load function $I_\mathrm{L}(v)$.

Proof: Consider the storage function S_L along with its time derivative

$$S_\mathrm{L} = \frac{C_\mathrm{eq}}{2} \tilde{v}^2 \tag{33}$$

$$\dot{S}_\mathrm{L} = -\tilde{v} \boldsymbol{e}_{\mathrm{P,r}}^\mathrm{T} \tilde{\boldsymbol{i}}_\mathrm{t} - \tilde{v} \tilde{I}_\mathrm{L}(\tilde{v}). \tag{34}$$

Since the static load function $I_\mathrm{L}(v)$ is IF-OFP according to Proposition 5, it is bounded from below by $\underline{c}_\mathrm{L} \tilde{v}^2 \leq \tilde{v} \tilde{I}_\mathrm{L}(\tilde{v})$ [see (6)]. Incorporate this lower bound into (34) to obtain

$$\dot{S}_\mathrm{L} \leq w_\mathrm{L} \coloneqq -\tilde{v} \boldsymbol{e}_{\mathrm{P,r}}^\mathrm{T} \tilde{\boldsymbol{i}}_\mathrm{t} - \underline{c}_\mathrm{L} \tilde{v}^2 \tag{35}$$

which yields the OFP property from Definition 2. ∎

Remark 9 (ZIP Load Passivity): Proposition 9 and (4) demonstrate that the passivity properties of the unactuated buses are directly linked to the smallest gradient of the load function. For the ZIP load in (16), this yields

$$\underline{c}_\mathrm{L} = \min\left(Z^{-1},\ Z^{-1} - \frac{P}{v_\mathrm{crit}^2},\ Z_\mathrm{crit}^{-1}\right). \tag{36}$$

Considering the strictly passive case ($\underline{c}_{\mathrm{L}} = 0$) along with $I, P \geq 0$ yields the passivity condition $Z^{-1} v_{\mathrm{crit}}^2 \geq P$ frequently used in the literature [10], [16], [18], [19], [20].

2) DGU Passivity: Shift the states (e, i, v) and inputs $(\phi^*, \boldsymbol{e}_{\mathrm{P,r}}^{\mathrm{T}} \boldsymbol{i}_{\mathrm{t}})$ of the DGU dynamics in (21) for the buses in $\mathcal{N}_\alpha$ to the respective error variables $(\tilde{e}, \tilde{i}, \tilde{v})$ and $(\tilde{\phi}^*, \boldsymbol{e}_{\mathrm{P,r}}^{\mathrm{T}} \tilde{\boldsymbol{i}}_{\mathrm{t}})$ to obtain (37), as shown at the bottom of the page, where the static load function is incorporated into the matrix $\boldsymbol{A}_{\mathrm{d}}$. Furthermore, the measured power $p = vi = v(\tilde{i} + \hat{i})$ in (19) is left partially in unshifted variables such that $\boldsymbol{A}_{\mathrm{d}}$ is also dependent on the unshifted voltage v and the steady-state current $\hat{i}$.

Note that the constant $\boldsymbol{\chi}_{\mathrm{d}}$ in (37) is found by setting the error variables $(\tilde{\phi}^*, \boldsymbol{e}_{\mathrm{P,r}}^{\mathrm{T}} \tilde{\boldsymbol{i}}_{\mathrm{t}}, \tilde{e}_{\mathrm{d}}, \tilde{i}, \tilde{v})$ and their time derivatives to zero. As such, the constant $\boldsymbol{\chi}_{\mathrm{d}} \equiv 0$ can be disregarded in the passivity analysis. We now analyze the shifted nonlinear system in (37) for EIP.

Theorem 10 (EIP DGUs): The shifted DGU dynamics in (37) are simultaneously IF-OFP($\nu_{\mathrm{d},1}, \rho_{\mathrm{d}}$) with respect to the input–output pair $(\tilde{\phi}^*, \tilde{v})$ and IFP($\nu_{\mathrm{d},2}$) with respect to the input–output pair $(-\boldsymbol{e}_{\mathrm{P,r}}^{\mathrm{T}} \tilde{\boldsymbol{i}}_{\mathrm{t}}, \tilde{v})$, if a feasible solution can be found for

$$\max_{\boldsymbol{P}_{\mathrm{d}},\, \nu_{\mathrm{d},1},\, \nu_{\mathrm{d},2},\, \rho_{\mathrm{d}}} \nu_{\mathrm{d},1} + \nu_{\mathrm{d},2} + \rho_{\mathrm{d}}$$
$$\text{s.t. (39) holds} \quad \forall v \in \mathcal{V} \subseteq \mathbb{R}_+ \ \forall \hat{i} \in \hat{\mathcal{I}} \subseteq \mathbb{R} \tag{38}$$

where $\boldsymbol{Q}_{\mathrm{d}}(v, \hat{i}, \underline{c}_{\mathrm{L}}) \coloneqq \boldsymbol{P}_{\mathrm{d}} \boldsymbol{A}_{\mathrm{d}}(v, \hat{i}, \underline{c}_{\mathrm{L}}) + \boldsymbol{A}_{\mathrm{d}}^{\mathrm{T}}(v, \hat{i}, \underline{c}_{\mathrm{L}}) \boldsymbol{P}_{\mathrm{d}}$

$$\boldsymbol{A}_{\mathrm{d}}(v, \hat{i}, \underline{c}_{\mathrm{L}}) = \begin{bmatrix} 0 & -v & -\hat{i} \\ k_{\mathrm{d}}^I & \tilde{R} - R - k_{\mathrm{d}}^P v & -1 - k_{\mathrm{u}}^P \hat{i} \\ 0 & 1 & -\underline{c}_{\mathrm{L}} \end{bmatrix} \tag{40}$$

and with $\nu_{\mathrm{d},1}, \nu_{\mathrm{d},2}, \rho_{\mathrm{d}} \in \mathbb{R}$, $\underline{c}_{\mathrm{L}}$ as in (4) and $\boldsymbol{c}_{\mathrm{d}} = [0, 0, 1]^{\mathrm{T}}$.

Proof: Consider, for (37), the storage function

$$S_{\mathrm{d}} = \begin{bmatrix} \tilde{e}_{\mathrm{d}} \\ \tilde{i} \\ \tilde{v} \end{bmatrix}^{\mathrm{T}} \boldsymbol{P}_{\mathrm{d}} \begin{bmatrix} \tilde{e}_{\mathrm{d}} \\ L\tilde{i} \\ C_{\mathrm{eq}} \tilde{v} \end{bmatrix} \tag{41}$$

with $\boldsymbol{P}_{\mathrm{d}} \succ 0$. The time derivative of (41) is

$$\dot{S}_{\mathrm{d}} = \begin{bmatrix} \tilde{\boldsymbol{x}}_{\mathrm{d}} \\ \tilde{\phi}^* \\ \boldsymbol{e}_{\mathrm{P,r}}^{\mathrm{T}} \tilde{\boldsymbol{i}}_{\mathrm{t}} \end{bmatrix}^{\mathrm{T}} \begin{bmatrix} \boldsymbol{Q}_{\mathrm{d}}\left(v, \hat{i}, \dfrac{\tilde{I}_{\mathrm{L}}(\tilde{v})}{\tilde{v}}\right) & \boldsymbol{P}_{\mathrm{d}} \boldsymbol{b}_{\mathrm{d},1}(\eta) & \boldsymbol{P}_{\mathrm{d}} \boldsymbol{b}_{\mathrm{d},2} \\ \boldsymbol{b}_{\mathrm{d},1}^{\mathrm{T}}(\eta) \boldsymbol{P}_{\mathrm{d}} & 0 & 0 \\ \boldsymbol{b}_{\mathrm{d},2}^{\mathrm{T}} \boldsymbol{P}_{\mathrm{d}} & 0 & 0 \end{bmatrix} \cdot \begin{bmatrix} \tilde{\boldsymbol{x}}_{\mathrm{d}} \\ \tilde{\phi}^* \\ \boldsymbol{e}_{\mathrm{P,r}}^{\mathrm{T}} \tilde{\boldsymbol{i}}_{\mathrm{t}} \end{bmatrix} \tag{42}$$

with $\tilde{\boldsymbol{x}}_{\mathrm{d}}$ as in (37). Since it follows from (6) that $-\tilde{v} \tilde{I}_{\mathrm{L}}(\tilde{v}) \leq -\underline{c}_{\mathrm{L}} \tilde{v}^2$, this bound can be incorporated into the inequality:

$$\dot{S}_{\mathrm{d}} \leq \begin{bmatrix} \tilde{\boldsymbol{x}}_{\mathrm{d}} \\ \tilde{\phi}^* \\ \boldsymbol{e}_{\mathrm{P,r}}^{\mathrm{T}} \tilde{\boldsymbol{i}}_{\mathrm{t}} \end{bmatrix}^{\mathrm{T}} \begin{bmatrix} \boldsymbol{Q}_{\mathrm{d}}(v, \hat{i}, \underline{c}_{\mathrm{L}}) & \boldsymbol{P}_{\mathrm{d}} \boldsymbol{b}_{\mathrm{d},1}(\eta) & \boldsymbol{P}_{\mathrm{d}} \boldsymbol{b}_{\mathrm{d},2} \\ \boldsymbol{b}_{\mathrm{d},1}^{\mathrm{T}}(\eta) \boldsymbol{P}_{\mathrm{d}} & 0 & 0 \\ \boldsymbol{b}_{\mathrm{d},2}^{\mathrm{T}} \boldsymbol{P}_{\mathrm{d}} & 0 & 0 \end{bmatrix} \begin{bmatrix} \tilde{\boldsymbol{x}}_{\mathrm{d}} \\ \tilde{\phi}^* \\ \boldsymbol{e}_{\mathrm{P,r}}^{\mathrm{T}} \tilde{\boldsymbol{i}}_{\mathrm{t}} \end{bmatrix}. \tag{43}$$

The desired IF-OFP and IFP properties for the DGU are described by the supply rate

$$w_{\mathrm{d}} = (1 + \nu_{\mathrm{d},1} \rho_{\mathrm{d}}) \tilde{\phi}^* \tilde{v} - \nu_{\mathrm{d},1} (\tilde{\phi}^*)^2 - \rho_{\mathrm{d}} \tilde{v}^2 - \tilde{v} \boldsymbol{e}_{\mathrm{P,r}}^{\mathrm{T}} \tilde{\boldsymbol{i}}_{\mathrm{t}} - \nu_{\mathrm{d},2} \left(\boldsymbol{e}_{\mathrm{P,r}}^{\mathrm{T}} \tilde{\boldsymbol{i}}_{\mathrm{t}}\right)^2. \tag{44}$$

These properties are guaranteed, if $\dot{S}_{\mathrm{d}} - w_{\mathrm{d}} < 0$ for all valid inputs and outputs and for $v \in \mathcal{V}$ and $\hat{i} \in \hat{\mathcal{I}}$. Combining (43) and (44) in this manner directly leads to constraint (39), as shown at the bottom of the page, in (38). Finally, the objective function in (38) seeks to find the largest indices for which the constraints are satisfied in a similar manner to Theorem 6. ■

Although Theorem 10 demonstrates the EIP of the actuated buses, notice that the $\tilde{e}_{\mathrm{d}}$ and $\hat{i}$ of (37) are not included in the supply rate w_{d} in (44). As such, an investigation of the zero state dynamics of the DGU is required.

Proposition 11 (ZSO DGUs): The shifted DGU dynamics in (37) are ZSO.

Proof: In (37), set the inputs $\tilde{\phi}^* \equiv 0$ and $\tilde{\boldsymbol{i}}_{\mathrm{t}} \equiv 0$ and the output $\tilde{v} \equiv 0$. Since $\boldsymbol{\chi}_{\mathrm{d}} = 0$ and $\tilde{I}_{\mathrm{L}}(0) = 0$,[8] verify from the

[8]This is a direct consequence of the shift according to (3).

$$\begin{bmatrix} \dot{\tilde{e}}_{\mathrm{d}} \\ L\dot{\tilde{i}} \\ C_{\mathrm{eq}} \dot{\tilde{v}} \end{bmatrix} = \underbrace{\begin{bmatrix} 0 & -v & -\hat{i} \\ k_{\mathrm{d}}^I & \tilde{R} - R - k_{\mathrm{d}}^P v & -1 - k_{\mathrm{u}}^P \hat{i} \\ 0 & 1 & -\dfrac{\tilde{I}_{\mathrm{L}}(\tilde{v})}{\tilde{v}} \end{bmatrix}}_{\boldsymbol{A}_{\mathrm{d}}(v, \hat{i}, \frac{\tilde{I}_{\mathrm{L}}(\tilde{v})}{\tilde{v}})} \underbrace{\begin{bmatrix} \tilde{e}_{\mathrm{d}} \\ \tilde{i} \\ \tilde{v} \end{bmatrix}}_{\tilde{\boldsymbol{x}}_{\mathrm{d}}} + \underbrace{\begin{bmatrix} 1 \\ k_{\mathrm{d}}^P \eta \\ 0 \end{bmatrix}}_{\boldsymbol{b}_{\mathrm{d},1}(\eta)} \tilde{\phi}^* - \underbrace{\begin{bmatrix} 0 \\ 0 \\ 1 \end{bmatrix}}_{\boldsymbol{b}_{\mathrm{d},2}} \boldsymbol{e}_{\mathrm{P,r}}^{\mathrm{T}} \tilde{\boldsymbol{i}}_{\mathrm{t}} + \underbrace{\begin{bmatrix} \eta \hat{\phi}^* - \hat{v} \hat{i} \\ k_{\mathrm{u}}^I \hat{e}_{\mathrm{d}} + (\tilde{R} - R) \hat{i} - \hat{v} + v_{\mathrm{Ref}} - k_{\mathrm{u}}^P (\eta \hat{\phi}^* - \hat{v} \hat{i}) \\ \hat{i} - \boldsymbol{e}_{\mathrm{P,r}}^{\mathrm{T}} \hat{\boldsymbol{i}}_{\mathrm{t}} - I_{\mathrm{L}}(\hat{v}) \end{bmatrix}}_{\boldsymbol{\chi}_{\mathrm{d}}} \tag{37}$$

$$\begin{bmatrix} \boldsymbol{Q}_{\mathrm{d}}(v, \hat{i}, \underline{c}_{\mathrm{L}}) + \rho_{\mathrm{d}} \boldsymbol{c}_{\mathrm{d}} \boldsymbol{c}_{\mathrm{d}}^{\mathrm{T}} & \boldsymbol{P}_{\mathrm{d}} \boldsymbol{b}_{\mathrm{d},1}(\eta) - \dfrac{1 + \nu_{\mathrm{d},1} \rho_{\mathrm{d}}}{2} \boldsymbol{c}_{\mathrm{d}} & \boldsymbol{P}_{\mathrm{d}} \boldsymbol{b}_{\mathrm{d},2} - \dfrac{1}{2} \boldsymbol{c}_{\mathrm{d}} \\ \boldsymbol{b}_{\mathrm{d},1}^{\mathrm{T}}(\eta) \boldsymbol{P}_{\mathrm{d}} - \dfrac{1 + \nu_{\mathrm{d},1} \rho_{\mathrm{d}}}{2} \boldsymbol{c}_{\mathrm{d}}^{\mathrm{T}} & \nu_{\mathrm{d},1} & 0 \\ \boldsymbol{b}_{\mathrm{d},2}^{\mathrm{T}} \boldsymbol{P}_{\mathrm{d}} - \dfrac{1}{2} \boldsymbol{c}_{\mathrm{d}}^{\mathrm{T}} & 0 & \nu_{\mathrm{d},2} \end{bmatrix} \prec 0, \quad \boldsymbol{P}_{\mathrm{d}} \succ 0 \tag{39}$$

equation for $\dot{\tilde{v}}$ that $\tilde{i} \equiv 0$. From the equation for $\dot{\tilde{i}}$, it then follows that $\tilde{e}_{\mathrm{d}} \equiv 0$, which concludes this proof. ■

Remark 10 (Compensating Nonpassive Loads): As demonstrated in [11], adding a term dependent on $\dot{v}_k$ to the regulator output $v_{\mathrm{s},k}$ in (19) allows for damping to be added to the unactuated state v_k. This, in turn, allows for regulation in the presence of nonpassive loads and can yield more favorable passivity indices when applying Theorem 10.

3) Line Passivity: The dynamics of the line subsystem (18) shifted to the equilibrium $(\hat{i}_{\mathrm{t}}, \hat{\boldsymbol{v}})$ yield

$$L_{\mathrm{t}}\dot{\tilde{i}}_{\mathrm{t}} = -R_{\mathrm{t}}\tilde{i}_{\mathrm{t}} + \boldsymbol{e}_{\mathrm{P,c}}^{\mathrm{T}}\tilde{\boldsymbol{v}} \tag{45}$$

which can now be analyzed for passivity.

Proposition 12 (OFP Lines): The shifted line dynamics in (45) are OFP(ρ_{t}), with $\rho_{\mathrm{t}} = R_{\mathrm{t}}$, with respect to the input–output pair $(\boldsymbol{e}_{\mathrm{P,c}}^{\mathrm{T}}\tilde{\boldsymbol{v}}, \tilde{i}_{\mathrm{t}})$ with the storage function

$$S_{\mathrm{t}} = \frac{L_{\mathrm{t}}}{2}\tilde{i}_{\mathrm{t}}^2. \tag{46}$$

Proof: The proof follows trivially by verifying that:

$$\dot{S}_{\mathrm{t}} = \tilde{i}_{\mathrm{t}}\boldsymbol{e}_{\mathrm{P,c}}^{\mathrm{T}}\tilde{\boldsymbol{v}} - R_{\mathrm{t}}\tilde{i}_{\mathrm{t}}^2 =: w_{\mathrm{t}} \tag{47}$$

where w_{t} in an OFP supply rate as per Definition 2. ■

4) Interconnected Microgrid Dissipativity: Having separately analyzed the subsystems comprising the microgrid, we now combine the results to formulate the dissipativity of the full microgrid with respect to the input–output pair $(\tilde{\boldsymbol{\phi}}^*, \tilde{\boldsymbol{v}})$. For simplicity, we group the buses according to their actuation states (13). Thus, $\tilde{\boldsymbol{\phi}}^* = [\tilde{\boldsymbol{\phi}}_{\alpha}^{*\mathrm{T}}, \tilde{\boldsymbol{\phi}}_{\beta}^{*\mathrm{T}}]^{\mathrm{T}}$ and $\tilde{\boldsymbol{v}} = [\tilde{\boldsymbol{v}}_{\alpha}^{\mathrm{T}}, \tilde{\boldsymbol{v}}_{\beta}^{\mathrm{T}}]^{\mathrm{T}}$ have the same dimensions. Note that we include the inputs $\tilde{\boldsymbol{\phi}}_{\beta}^*$ for the unactuated buses in $\mathcal{N}_{\beta}$ as provided by the four-stage controller (see Fig. 2) even though these inputs are not used.

Proposition 13 (Microgrid Dissipativity): A dc microgrid comprising DGUs (21), lines (18), and loads (15) with an interconnection topology described by a connected graph $\mathcal{G}_{\mathrm{P}}$ is dissipative with respect to the supply rate

$$\begin{aligned} w_{\mathrm{M},\alpha\beta} = (1 + \nu_{\mathrm{d},1}\rho_{\mathrm{d}})\tilde{\boldsymbol{\phi}}_{\alpha}^{*\mathrm{T}}\tilde{\boldsymbol{v}}_{\alpha} - \nu_{\mathrm{d},1}\tilde{\boldsymbol{\phi}}_{\alpha}^{*\mathrm{T}}\tilde{\boldsymbol{\phi}}_{\alpha}^{*} \\ - \rho_{\mathrm{d}}\tilde{\boldsymbol{v}}_{\alpha}^{\mathrm{T}}\tilde{\boldsymbol{v}}_{\alpha} - \rho_{\mathrm{L}}\tilde{\boldsymbol{v}}_{\beta}^{\mathrm{T}}\tilde{\boldsymbol{v}}_{\beta} \end{aligned} \tag{48}$$

if $\nu_{\mathrm{d},2} + \rho_{\mathrm{t}} \geq 0$ for the worst-case indices of the buses and lines calculated in Proposition 9 (ρ_{L}), Proposition 12 (ρ_{t}), and Theorem 10 ($\nu_{\mathrm{d},1}$, $\nu_{\mathrm{d},2}$, ρ_{d}), i.e.,

$$\begin{aligned} \nu_{\mathrm{d},1} &= \min_{k\in\mathcal{N}_{\alpha}} \nu_{\mathrm{d},1,k}, \quad \nu_{\mathrm{d},2} = \min_{k\in\mathcal{N}_{\alpha}} \nu_{\mathrm{d},2,k}, \quad \rho_{\mathrm{d}} = \min_{k\in\mathcal{N}_{\alpha}} \rho_{\mathrm{d},k} \\ \rho_{\mathrm{L}} &= \min_{k\in\mathcal{N}_{\beta}} \rho_{\mathrm{L},k}, \quad \rho_{\mathrm{t}} = \min_{kl\in\mathcal{E}_{\mathrm{P}}} \rho_{\mathrm{t},k}. \end{aligned} \tag{49}$$

Proof: Define, for the interconnected microgrid, the storage function

$$S_{\mathrm{M}} = \sum_{k\in\mathcal{N}_{\alpha}} S_{\mathrm{d},k} + \sum_{k\in\mathcal{N}_{\beta}} S_{\mathrm{L},k} + \sum_{kl\in\mathcal{E}_{\mathrm{P}}} S_{\mathrm{t},kl}. \tag{50}$$

An upper bound for time derivative of (50) may then be found by combining the supply rates in (35), (44), and (47)

$$\begin{aligned} \dot{S}_{\mathrm{M}} \leq\ & (1 + \nu_{\mathrm{d},1}\rho_{\mathrm{d}})\tilde{\boldsymbol{\phi}}_{\alpha}^{*\mathrm{T}}\tilde{\boldsymbol{v}}_{\alpha} - \nu_{\mathrm{d},1}\tilde{\boldsymbol{\phi}}_{\alpha}^{*\mathrm{T}}\tilde{\boldsymbol{\phi}}_{\alpha}^{*} - \rho_{\mathrm{d}}\tilde{\boldsymbol{v}}_{\alpha}^{\mathrm{T}}\tilde{\boldsymbol{v}}_{\alpha} \\ & + \tilde{\boldsymbol{i}}_{\mathrm{t}}^{\mathrm{T}}\boldsymbol{E}^{\mathrm{T}}\tilde{\boldsymbol{v}} - \tilde{\boldsymbol{v}}_{\alpha}^{\mathrm{T}}\boldsymbol{E}_{\alpha}\tilde{\boldsymbol{i}}_{\mathrm{t}} - \tilde{\boldsymbol{v}}_{\beta}^{\mathrm{T}}\boldsymbol{E}_{\beta}\tilde{\boldsymbol{i}}_{\mathrm{t}} \\ & - \rho_{\mathrm{L}}\tilde{\boldsymbol{v}}_{\beta}^{\mathrm{T}}\tilde{\boldsymbol{v}}_{\beta} - (\nu_{\mathrm{d},2} + \rho_{\mathrm{t}})\tilde{\boldsymbol{i}}_{\mathrm{t}}^{\mathrm{T}}\tilde{\boldsymbol{i}}_{\mathrm{t}}. \end{aligned} \tag{51}$$

The interconnection of the nodes and lines results in $\tilde{\boldsymbol{i}}_{\mathrm{t}}^{\mathrm{T}}\boldsymbol{E}^{\mathrm{T}}\tilde{\boldsymbol{v}} = \tilde{\boldsymbol{v}}_{\alpha}^{\mathrm{T}}\boldsymbol{E}_{\alpha}\tilde{\boldsymbol{i}}_{\mathrm{t}} + \tilde{\boldsymbol{v}}_{\beta}^{\mathrm{T}}\boldsymbol{E}_{\beta}\tilde{\boldsymbol{i}}_{\mathrm{t}}$. Furthermore with $\nu_{\mathrm{d},2} + \rho_{\mathrm{t}} \geq 0$, we can drop the unnecessary strictly negative $\tilde{\boldsymbol{i}}_{\mathrm{t}}^{\mathrm{T}}\tilde{\boldsymbol{i}}_{\mathrm{t}}$ term and verify that $\dot{S}_{\mathrm{M}} \leq w_{\mathrm{M},\alpha\beta}$. ■

Through Proposition 13, the dissipativity of the entire microgrid is formulated using the desired input and output vectors. However, the supply rate in (48) is dependent on the actuation states of the buses. We now remove this dependence by finding a supply rate for a specific bus that encompasses both its actuated and unactuated states. By considering a quadratic supply rate as a sector condition (see [26], [29]), a combined supply rate is found through the union of the sectors for the actuated and unactuated cases.

Theorem 14 (Actuation-Independent Passivity): A dc microgrid for which Proposition 13 holds is IF-OFP($\nu_{\mathrm{d},1}$, ρ_{d}) with respect to the supply rate

$$w_{\mathrm{M}} = (1 + \nu_{\mathrm{d},1}\rho_{\mathrm{d}})\tilde{\boldsymbol{\phi}}^{*\mathrm{T}}\tilde{\boldsymbol{v}} - \nu_{\mathrm{d},1}\tilde{\boldsymbol{\phi}}^{*\mathrm{T}}\tilde{\boldsymbol{\phi}}^{*} - \rho_{\mathrm{d}}\tilde{\boldsymbol{v}}^{\mathrm{T}}\tilde{\boldsymbol{v}} \tag{52}$$

if the following conditions hold:

$$0 \leq \nu_{\mathrm{d},2} + \rho_{\mathrm{t}} \tag{53}$$

$$0 < \rho_{\mathrm{L}} < 1 \tag{54}$$

$$0 > \nu_{\mathrm{d},1}. \tag{55}$$

The proof of Theorem 14 can be found in Appendix A. Through (52), we, thus, show that a single IF-OFP supply rate describes the input–output passivity of the entire microgrid, irrespective of the states of actuation of the buses. This supply rate is derived from the properties of the DGUs in Theorem 10 and accounts for the worst case loads.

Remark 11 (Nonpassive Loads at DGUs): While (54) in Theorem 14 requires strictly passive loads at unactuated buses, this is not required for the loads at actuated buses. Indeed, the loads at DGUs may exhibit a lack of passivity with $\underline{c}_{\mathrm{L}} < 0$. However, this would be reflected by the indices obtained in Theorem 10 and the supply rate in (52).

Remark 12 (Nonstatic Loads): Due to the use of passivity in this section, the analysis presented here effortlessly extends to the case of dynamic loads. Such dynamic loads simply need to exhibit equivalent IFP properties (see Proposition 9) and must be ZSO.

Remark 13 (Analytical Microgrid Supply Rate): The analytically derived dc microgrid supply rate in Theorem 14, based on the worst-case numerically derived DGU supply rate (see Theorem 10), is scalable and topology-independent. Furthermore, other controllers using the same port $(\tilde{\boldsymbol{v}}, \tilde{\boldsymbol{\phi}}^*)$ can directly use the supply rate in (52) for a stability analysis. Examples include controllers using interconnection and damping assignment passivity-based control [24, p. 190] or passivity-based model predictive control (see [36]).

B. Controller EIP

Having analyzed the passivity of the microgrid subsystems and their interconnection, we now investigate the passivity properties of the control structure in Section IV. This is done successively for each part of the controller: the DDA stages, the PI stage, and the weighting function.

1) DDA EIP: Consider the DDA stages in Fig. 2 shifted to their equilibria, i.e., with $\tilde{\boldsymbol{u}}_{\mathrm{a},s}$, $\tilde{\boldsymbol{x}}_{\mathrm{a},s}$, $\tilde{\boldsymbol{z}}_{\mathrm{a},s}$, and $\tilde{\boldsymbol{y}}_{\mathrm{a},s}$. As shown in [34], each DDA has an unobservable and uncontrollable mode $\varkappa_{\mathrm{a},s}$ with zero dynamics, such that

$$\tilde{\boldsymbol{z}}_{\mathrm{a},s} = \begin{bmatrix} \boldsymbol{\tau}_{\mathrm{a}} & \boldsymbol{T}_{\mathrm{a}} \end{bmatrix} \begin{bmatrix} \tilde{\varkappa}_{\mathrm{a},s} \\ \tilde{\boldsymbol{\xi}}_{\mathrm{a},s} \end{bmatrix} \tag{56}$$

where $\boldsymbol{\tau}_{\mathrm{a}}$ is the left unit eigenvector of $\boldsymbol{\mathcal{L}}_{\mathrm{C}}$ such that $\boldsymbol{\mathcal{L}}_{\mathrm{C}}^{\mathrm{T}}\boldsymbol{\tau}_{\mathrm{a}} = \boldsymbol{0}$ and where $\boldsymbol{T}_{\mathrm{a}}$ are the remaining $N-1$ left unit eigenvectors.

Proposition 15 (DDA EIP): The DDA controller in (24) shifted to its equilibrium with the storage function

$$S_{\mathrm{a},s} = \frac{1}{2\gamma_{\mathrm{a}}}\left(\tilde{\boldsymbol{x}}_{\mathrm{a},s}^{\mathrm{T}}\tilde{\boldsymbol{x}}_{\mathrm{a},s} + \tilde{\boldsymbol{z}}_{\mathrm{a},s}^{\mathrm{T}}\tilde{\boldsymbol{z}}_{\mathrm{a},s}\right) \tag{57}$$

is OFP(ρ_{a}), $\rho_{\mathrm{a}} = 1$, with respect to $(\tilde{\boldsymbol{u}}_{\mathrm{a},s}, \tilde{\boldsymbol{y}}_{\mathrm{a},s})$. Moreover, the reduced DDA, obtained by dropping mode $\tilde{\varkappa}_{\mathrm{a},s}$, is ZSO.

Proof: The time derivative of (57) is

$$\begin{aligned} \dot{S}_{\mathrm{a},s} &= -\tilde{\boldsymbol{x}}_{\mathrm{a},s}^{\mathrm{T}}\tilde{\boldsymbol{x}}_{\mathrm{a},s} - \frac{1}{\gamma_{\mathrm{a}}}\tilde{\boldsymbol{x}}_{\mathrm{a},s}^{\mathrm{T}}\boldsymbol{\mathcal{L}}_{\mathrm{C},P}\tilde{\boldsymbol{x}}_{\mathrm{a},s} + \tilde{\boldsymbol{x}}_{\mathrm{a},s}^{\mathrm{T}}\tilde{\boldsymbol{u}}_{\mathrm{a},s} \\ &\leq w_{\mathrm{a},s} \coloneqq \tilde{\boldsymbol{x}}_{\mathrm{a},s}^{\mathrm{T}}\tilde{\boldsymbol{u}}_{\mathrm{a},s} - \tilde{\boldsymbol{x}}_{\mathrm{a},s}^{\mathrm{T}}\tilde{\boldsymbol{x}}_{\mathrm{a},s} \end{aligned} \tag{58}$$

since $\boldsymbol{\mathcal{L}}_{\mathrm{C},P} \succcurlyeq 0$ and $\gamma_{\mathrm{a}} > 0$, thus verifying the OFP property for $\tilde{\boldsymbol{y}}_{\mathrm{a},s} = \tilde{\boldsymbol{x}}_{\mathrm{a},s}$. To show ZSO of the reduced DDA, set $\tilde{\boldsymbol{u}}_{\mathrm{a},s} \equiv \tilde{\boldsymbol{y}}_{\mathrm{a},s} \equiv \boldsymbol{0}$. From (24), we see that $\tilde{\boldsymbol{x}}_{\mathrm{a},s} \equiv \boldsymbol{0}$ and $\boldsymbol{\mathcal{L}}_{\mathrm{C},I}^{\mathrm{T}}\tilde{\boldsymbol{z}}_{\mathrm{a},s} = \boldsymbol{0}$. Through (56) and since $\mathrm{rank}[\boldsymbol{\mathcal{L}}_{\mathrm{C},I}^{\mathrm{T}}\boldsymbol{T}_{\mathrm{a}}] = N-1$ and $\boldsymbol{\mathcal{L}}_{\mathrm{C},I}^{\mathrm{T}}\boldsymbol{\tau}_{\mathrm{a}} = \boldsymbol{0}$, we find that $\tilde{\boldsymbol{\xi}}_{\mathrm{a},s} = \boldsymbol{0}$ but the mode with zero dynamics $\tilde{\varkappa}_{\mathrm{a},s}$ is free. Thus, by dropping the unobservable and uncontrollable mode with zero dynamics, we obtain a reduced DDA that is ZSO. ∎

The OFP result in Proposition 15 also means that (24) has an L_2-gain of 1 [28, p. 3].

Remark 14 (DDA Convergence): The result in Proposition 15 guarantees that $\lim_{t\to\infty}\tilde{\boldsymbol{x}}_{\mathrm{a},s} = \boldsymbol{0}$ and $\lim_{t\to\infty}\tilde{\boldsymbol{\xi}}_{\mathrm{a},s} = \boldsymbol{0}$ if the DDA input–output port is connected in a passivity preserving way. Even though the ZSO property does not include the mode $\tilde{\varkappa}_{\mathrm{a},s}$, we know that $\dot{\tilde{\varkappa}}_{\mathrm{a},s} = 0$ and $\tilde{\varkappa}_{\mathrm{a},s}$ does not influence the states $\tilde{\boldsymbol{x}}_{\mathrm{a},s}$ and $\tilde{\boldsymbol{\xi}}_{\mathrm{a},s}$ (see [34]). The full DDA, therefore, has an asymptotically stable equilibrium manifold $\hat{\mathcal{X}}_{\mathrm{a},s} = \{\tilde{\boldsymbol{x}}_{\mathrm{a},s} = \boldsymbol{0}, \tilde{\boldsymbol{\xi}}_{\mathrm{a},s} = \boldsymbol{0}, \tilde{\varkappa}_{\mathrm{a},s} \in \mathbb{R}\}$.

2) PI EIP: Consider the PI controller in (27) shifted to its equilibrium, i.e., with $\tilde{\boldsymbol{u}}_{\mathrm{u}}$, $\tilde{\boldsymbol{x}}_{\mathrm{u}}$, and $\tilde{\boldsymbol{y}}_{\mathrm{u}}$. The ideal case with $\zeta_{\mathrm{u}} = 0$ can trivially be shown to be IFP(k_{u}^P) for the storage function $S_{\mathrm{u}} = k_{\mathrm{u}}^I\tilde{\boldsymbol{x}}_{\mathrm{u}}^{\mathrm{T}}\tilde{\boldsymbol{x}}_{\mathrm{u}}/2$. The leaky PI control with $\zeta_{\mathrm{u}} > 0$ exhibits the following properties.

Proposition 16 (Leaky PI EIP): The leaky PI control in (27) shifted to its equilibrium with the storage function $S_{\mathrm{u}} = k_{\mathrm{u}}^I\tilde{\boldsymbol{x}}_{\mathrm{u}}^{\mathrm{T}}\tilde{\boldsymbol{x}}_{\mathrm{u}}/2$ is dissipative with respect to

$$\begin{aligned} w_{\mathrm{u}} = \underbrace{\left(1+\frac{2\zeta_{\mathrm{u}}k_{\mathrm{u}}^P}{k_{\mathrm{u}}^I}\right)}_{2\sigma_{\mathrm{u}}}\tilde{\boldsymbol{u}}_{\mathrm{u}}^{\mathrm{T}}\tilde{\boldsymbol{y}}_{\mathrm{u}} - \underbrace{\left(k_{\mathrm{u}}^P + \frac{\zeta_{\mathrm{u}}k_{\mathrm{u}}^{P\,2}}{k_{\mathrm{u}}^I}\right)}_{\nu_{\mathrm{u}}}\tilde{\boldsymbol{u}}_{\mathrm{u}}^{\mathrm{T}}\tilde{\boldsymbol{u}}_{\mathrm{u}} \\ - \underbrace{\frac{\zeta_{\mathrm{u}}}{k_{\mathrm{u}}^I}}_{\rho_{\mathrm{u}}}\tilde{\boldsymbol{y}}_{\mathrm{u}}^{\mathrm{T}}\tilde{\boldsymbol{y}}_{\mathrm{u}}. \end{aligned} \tag{59}$$

Proof: Calculate the time derivative of S_{u} as $\dot{S}_{\mathrm{u}} = k_{\mathrm{u}}^I\tilde{\boldsymbol{x}}_{\mathrm{u}}^{\mathrm{T}}\tilde{\boldsymbol{u}}_{\mathrm{u}} - \zeta_{\mathrm{u}}k_{\mathrm{u}}^I\tilde{\boldsymbol{x}}_{\mathrm{u}}^{\mathrm{T}}\tilde{\boldsymbol{x}}_{\mathrm{u}}$. Substitute in $k_{\mathrm{u}}^I\tilde{\boldsymbol{x}}_{\mathrm{u}} = \tilde{\boldsymbol{y}}_{\mathrm{u}} - k_{\mathrm{u}}^P\tilde{\boldsymbol{u}}_{\mathrm{u}}$ from the output in (27) and simplify to verify that $\dot{S}_{\mathrm{u}} = w_{\mathrm{u}}$. ∎

Note that while w_{u} in (59) has a quadratic form, it does not directly match the IF-OFP form in Definition 2. However, by appropriately weighing the storage function S_{u}, the form in Definition 2 is easily obtained. Furthermore, since the supply rate is weighted by the free parameter d_3 in the sequel (see also Theorem 6), we omit this step for simplicity without affecting the results in the sequel.

3) Weighting Function EIP: The derivative of the weighting function in (29) is described by (see Fig. 3)

$$\frac{dy_{\mathrm{w}}}{du_{\mathrm{w}}} = a_{\mathrm{w}} + b_{\mathrm{w}}\tanh^2(g_{\mathrm{w}}(u_{\mathrm{w}})). \tag{60}$$

By setting $b_{\mathrm{w}} > -a_{\mathrm{w}}$ and applying Proposition 5, (29) is found to be IF-OFP($\nu_{\mathrm{w}}, \rho_{\mathrm{w}}$) with

$$\nu_{\mathrm{w}} = a_{\mathrm{w}}, \quad \rho_{\mathrm{w}} = \frac{1}{a_{\mathrm{w}} + b_{\mathrm{w}}}. \tag{61}$$

VI. Interconnected Stability

Using the passivity properties of the microgrid and controller subsystems obtained in Section V, we now investigate the stability of the microgrid and controller interconnected as in Fig. 2. However, we note that the agent PI controller and the Stage-4 DDA controller exhibit a cascaded IFP–OFP obstacle (see Proposition 7) if the PI controller is ideal ($\zeta_{\mathrm{u}} = 0$), which prevents a closed-loop analysis with dissipativity. Thus, in Section VI-A, we derive stability conditions using leaky agent PI controllers with $\zeta_{\mathrm{u}} > 0$.

A. Leaky PI-Controlled Stability

Consider the case where the passivity properties of all subsystems in Fig. 2 except for the weighting function (29) are fixed. Combining the results in Section V with Theorem 6, we now determine the weighting function parameters that guarantee closed-loop stability for the equilibrium manifold (see Remark 14).

Theorem 17 (Designed Closed-Loop Stability): The closed loop in Fig. 2 is guaranteed to be asymptotically stable for the weighting function parameters $a_{\mathrm{w}} = \nu_{\mathrm{w}}$, $b_{\mathrm{w}} = 1/\rho_{\mathrm{w}} - a_{\mathrm{w}}$ if a feasible solution is found for

$$\begin{aligned} \min_{\nu_{\mathrm{w}},\,\rho_{\mathrm{w}},\,d_i} \quad & \nu_{\mathrm{w}} + \rho_{\mathrm{w}} \\ \text{s.t.} \quad & \boldsymbol{Q} \prec 0, \quad d_i > 0, \ i = 1,\ldots,5 \end{aligned} \tag{62}$$

where $\sigma_{\mathrm{w}} = (1/2)(1+\nu_{\mathrm{w}}\rho_{\mathrm{w}})$, $\sigma_{\mathrm{d}} = (1/2)(1+\nu_{\mathrm{d},1}\rho_{\mathrm{d}})$, and

$$\boldsymbol{Q} = \begin{bmatrix} -\rho_{\mathrm{w}}d_1 & \frac{d_2}{2} & 0 & 0 & -\sigma_{\mathrm{w}}d_1 \\ \frac{d_2}{2} & -\rho_{\mathrm{a}}d_2 - \nu_{\mathrm{u}}d_3 & \sigma_{\mathrm{u}}d_3 & 0 & 0 \\ 0 & \sigma_{\mathrm{u}}d_3 & -\rho_{\mathrm{u}}d_3 & \frac{d_4}{2} & 0 \\ 0 & 0 & \frac{d_4}{2} & -\rho_{\mathrm{a}}d_4 - \nu_{\mathrm{d},1}d_5 & \sigma_{\mathrm{d}}d_5 \\ -\sigma_{\mathrm{w}}d_1 & 0 & 0 & \sigma_{\mathrm{d}}d_5 & -\rho_{\mathrm{d}}d_5 - \nu_{\mathrm{w}}d_1 \end{bmatrix}. \tag{63}$$

Proof: Use the supply rates for the dc microgrid in (52), the two DDA controllers in (58), the agent PI controller in (59), and the IF-OFP supply rate for the weighting function (61)

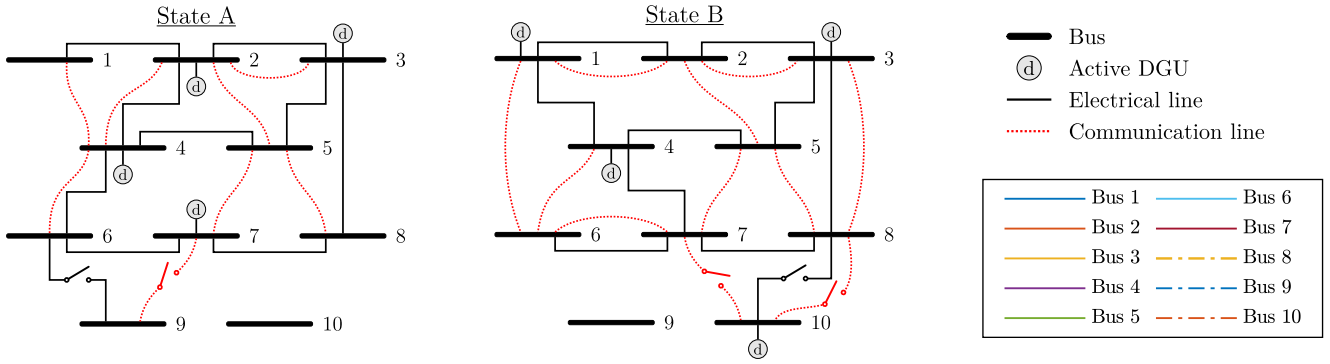

Fig. 4. Two different states for a ten-bus dc microgrid along with electrical and communication connections. The loads at the buses are omitted for clarity.

to construct $\boldsymbol{W}$ in (10). The five subsystems in Fig. 2 are interconnected by $\boldsymbol{u} = \boldsymbol{H}\,\boldsymbol{y}$, where

$$\boldsymbol{H} = \begin{bmatrix} 0 & 0 & 0 & 0 & -1 \\ 1 & 0 & 0 & 0 & 0 \\ 0 & 1 & 0 & 0 & 0 \\ 0 & 0 & 1 & 0 & 0 \\ 0 & 0 & 0 & 1 & 0 \end{bmatrix}. \tag{64}$$

Apply Theorem 6, with $\boldsymbol{D}$ as in (9) and simplify $\boldsymbol{Q}$ in (8) to obtain (63). This yields the optimization problem (62), where the indices of the weighting function $(\nu_{\mathrm{w}}, \rho_{\mathrm{w}})$ are configurable. Asymptotic stability is ensured by ensuring that any states not present in $\boldsymbol{y}$ are asymptotically stable. The latter condition is ensured through the zero-state analyses in Proposition 11, Proposition 15, and Remark 14, and through the condition in Proposition 13. Finally, the parameters a_{w} and b_{w} are calculated from (61). ■

Through the application of Theorem 17, the parameters for the weighting function can, thus, be designed to ensure stability. We highlight that the results in Section V and Theorem 17 hold irrespective of the physical or communication topologies and are independent of the actuation states of the nodes, as long as Assumptions 2 and 3 hold. Therefore, verifying Theorem 17 ensures robustness against any changes, which do not alter the worst-case passivity indices of the respective subsystems [see (49)]. Note that the optimization problem in Theorem 17 is complex and nonlinear, but is easy to verify. Additionally, $\boldsymbol{Q} \in \mathbb{R}^{5\times 5}$ in (63) has a fixed size that is independent of the size of the network.

VII. Simulation

In this section, we demonstrate the coordination and robustness of the proposed control structure by means of a MATLAB/Simulink simulation using Simscape components. We consider the network comprising ten buses depicted in Fig. 4. In Section VII-A, we describe the setup of the simulation along with the various changes that the network is subjected to. Next, in Section VII-B, simulation results are presented for the case where Theorem 17 holds, i.e., with strictly passive loads and leaky agent PI controllers. Finally, in Section VII-C, we show the robust stability of the proposed control structure for passive loads and ideal agent PI controllers.

TABLE I
Simulation Parameter Values

Voltages	$v_{\mathrm{Ref}} = 380\,\mathrm{V}$	$v_{\mathrm{crit}} = 266\,\mathrm{V}$
DGU Filters (14)	$R_k = 0.2\,\Omega$	$L_k = 1.8\,\mathrm{mH}$
	$C_k = 2.2\,\mathrm{mF}$	
ZIP Loads (16)	$\lvert Z^{-1}\rvert \leq 0.1/\Omega$	$\lvert I\rvert \leq 21\,\mathrm{A}$
	$\lvert P\rvert \leq 3\,\mathrm{kW}$	
Elec. Lines (18)	$R_{\mathrm{t},kl} = 0.1\,\Omega/\mathrm{km}$	$L_{\mathrm{t},kl} = 2\,\mu\mathrm{H/km}$
	$C_{\mathrm{t},kl} = 22\,\mathrm{nF/km}$	length $\in [0.1; 10]\,\mathrm{km}$

A. Simulation Setup

The dc microgrid in Fig. 4 is simulated with the parameters in Table I. The ZIP load parameters are chosen randomly in the specified ranges such that the required passivity measures are fulfilled (see Remark 9). Furthermore, typical values are used for the DGUs and the lines [4], [9], [13]. The lines exhibit the same per kilometer parameter values, and the line length is chosen randomly in the given interval. The line lengths are given in Appendix B. The power gains for the actuated buses are set to $\eta_1 = 0.8$, $\eta_2 = 1.0$, $\eta_3 = 1.2$, $\eta_4 = 1.4$, $\eta_7 = 1.6$, and $\eta_{10} = 0.6$.

The simulation starts off in State A (see Fig. 4) with Bus 9 connected and with all states at zero. The following changes are made at the indicated times.

1) $t = 5$ s: The actuation states α_i of the buses switch from State A to State B, and Bus 9 is disconnected.
2) $t = 10$ s: The communication topology switches from State A to State B, and Bus 10 is connected.
3) $t = 15$ s: The electrical topology switches from State A to State B.
4) $t = 20$ s: The bus actuation status along with the communication and electrical topologies revert to State A. Bus 9 is connected and Bus 10 is disconnected.

Furthermore, at each change, half of the buses are randomly selected and assigned new ZIP load parameters. The ZIP load parameters can be found in Appendix B.

The closed-loop controller parameters in Table II are designed successively, starting from the microgrid subsystems. First, the passivity indices for the lines ($\rho_{\mathrm{t}} = 0.01$) and loads ($\rho_{\mathrm{L}} = \varsigma_{\mathrm{L}} = 0.05$) are calculated from Proposition 12 and Proposition 9, respectively. Next, the parameters for the power regulator (19) are chosen to provide a fast and damped

TABLE II
CONTROLLER PARAMETER VALUES

Power PI Control (19)	$k_{\mathrm{d}}^P = 90$	$k_{\mathrm{d}}^I = 90$	$\tilde{R} = -8$
DDA Control (24)	$k_{\mathrm{a}}^P = 50$	$k_{\mathrm{a}}^I = 100$	$\gamma_{\mathrm{a}} = 16$
Agent PI Control (27)	$k_{\mathrm{u}}^P = 160$	$k_{\mathrm{u}}^I = 600$	$\zeta_{\mathrm{u}} = 0.08$
Weighting Function (29)	$a_{\mathrm{w}} = 0.1$	$b_{\mathrm{w}} = 1.1$	$c_{\mathrm{w}} = 7.5\,\mathrm{V}$

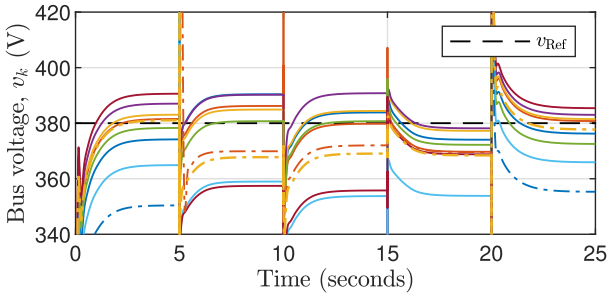

Fig. 5. Simulated bus voltages with line colors as per the legend in Fig. 4.

response (here, yielding a 5% settling time of 23 ms). Note that since the controllers (19), (24), and (27) all have a PI structure, conventional tuning methods may be applied. The DGU passivity indices are then calculated from Theorem 10, with the optimization verified for the practically relevant intervals $v \in [200\ \mathrm{V}, 550\ \mathrm{V}]$ and $\hat{i} \in [10\ \mathrm{A}, 350\ \mathrm{A}]$, and for a gain $\eta \in [0.6; 1.6]$. Note that adding the restriction $\nu_{\mathrm{d},2} \geq -\rho_{\mathrm{t}}$ to the optimization in Theorem 10 ensures that (53) will be met. This yields a worst-case solution $\nu_{\mathrm{d},1} = -4.696$, $\nu_{\mathrm{d},2} = -0.01$, and $\rho_{\mathrm{d}} = 0.01$, with which the microgrid supply rate is constructed as per Theorem 14. The DDA parameters have no effect on its passivity properties and thus do not influence the stability of the closed loop (see Proposition 15). Thus, its parameters were chosen to provide quick settling and disturbance rejection times (here, yielding a 5% settling time of 190 ms). Next, parameters for the agent PI controllers are found using the closed loop with the weighting function set to a unity gain (here, yielding a 5% settling of around 1.5 s). Finally, the weighting function parameters are designed using Theorem 17. Note that Theorem 14 requires strictly passive loads ($\underline{c}_{\mathrm{L}} > 0$) and Theorem 17 necessitates leaky integrators ($\zeta_{\mathrm{u}} > 0$).

B. Results

The bus voltages v_k shown in Fig. 5 confirm the stability of the closed-loop results although the voltages tend to be lower than desired, due to the use of leaky integrators. The remaining steady-state offset can also be seen in the weighted errors plotted in Fig. 6, where the average tends toward a nonzero value in each instance (see Remark 5). Despite this, the four-stage controller reaches a consensus on the average of the nonlinear weighted voltage errors. Note that the voltages of Buses 9 and 10 are at 0 V during the periods where they are disconnected and not actuated.

In Fig. 7, the outputs of the agent controllers show that no synchronization of the agent controllers is required or takes place. The agent controller outputs at Buses 1–8, which are continuously connected to the communication network, are

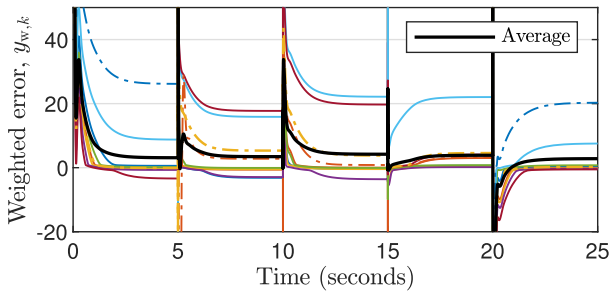

Fig. 6. Simulated weighted voltage errors and the average error of connected agents with agent line colors as per the legend in Fig. 4.

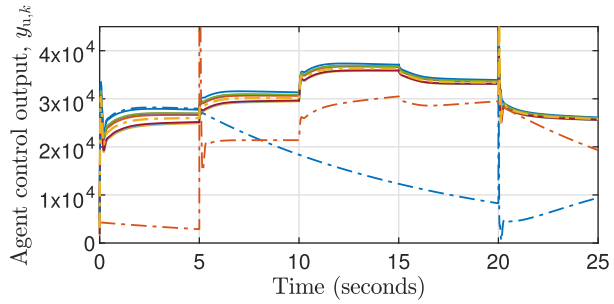

Fig. 7. Simulated outputs of the local agent controllers with line colors as per the legend in Fig. 4.

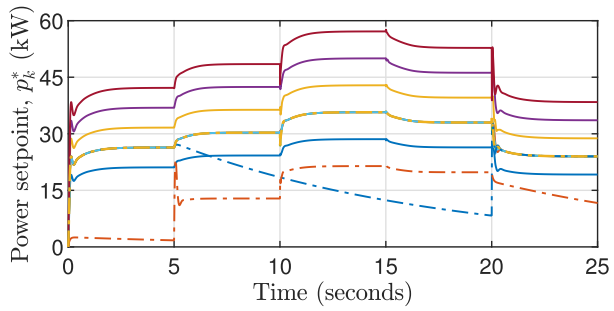

Fig. 8. Simulated power setpoints with line colors as per the legend in Fig. 4.

near identical. However, the disconnecting buses, e.g., Bus 9 after $t = 5$ s, rapidly diverge from other controllers and do not synchronize on reconnect. Nevertheless, the final controller stage ensures proportional cooperation, as demonstrated by the power setpoints $p_k^* = \eta_k \phi_k^*$ in Fig. 8. When Bus 10 connects at $t = 10$ s, its setpoint p_k^* rapidly converges to be proportional to the coordinated common setpoint used by all connected agents.

Although the leaky integrators yield imperfect results (see Remark 5 and Fig. 6), this can be mitigated by choosing a higher v_{Ref}. Indeed, by combining the steady state of the agent PI controller (28) with the DDA steady state (25), we see that injecting power into the system $p_k^* > 0$ results in positive voltage errors. Since we consider (strictly) passive loads, increasing v_{Ref} is, thus, a viable method for correcting the imperfect results while retaining the advantageous properties of the stability analysis in Theorem 17.

C. Robustness Test

We now repeat the simulation described in Section VII-A with the same random seed but with the following changes:

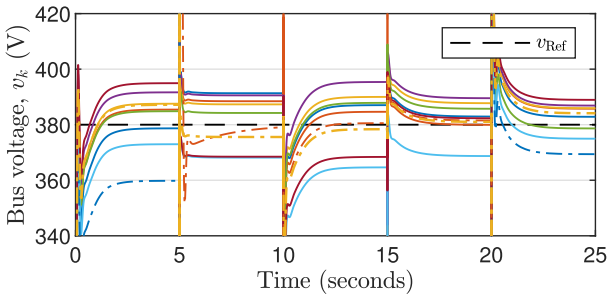

Fig. 9. Simulated bus voltages with ideal PI controllers and with line colors as per the legend in Fig. 4.

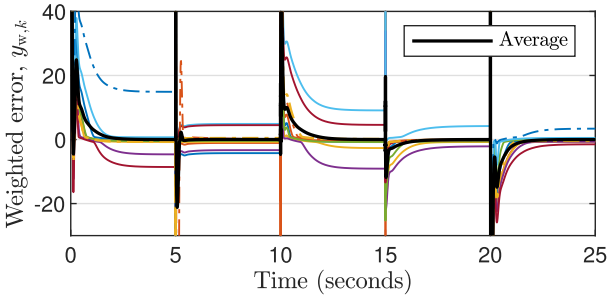

Fig. 10. Simulated weighted voltage errors and the average error of connected agents with ideal PI controllers and with agent line colors as per the legend in Fig. 4.

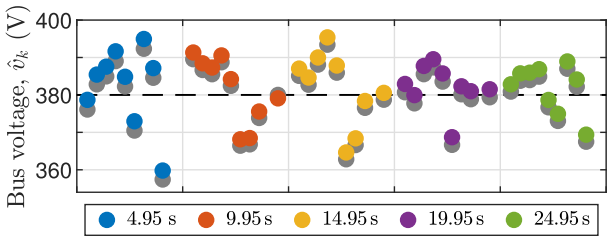

Fig. 11. Steady-state voltages of connected buses using the nonlinear weighting function (29) (colored) and a linear weighting (gray).

1) passive loads with $\underline{c}_{\text{L}} = 0$ are allowed at all buses and 2) ideal agent PI controllers with $\zeta_{\text{u}} = 0$ are used. Under these conditions, Theorem 17 can no longer be used to verify the stability. However, the stability can still be verified using classical approaches such as evaluating the eigenvalues for the linearized closed loop.

Fig. 9 demonstrates the improved regulation achieved by the ideal PI agents, in that the bus voltages are closer to v_{Ref} at steady state than in Fig. 5. Moreover, Fig. 10 shows that perfect regulation is achieved, where the average weighted error tends to zero in each case. Fig. 10 also demonstrates the robustness against communication interruptions, as is the case for Bus 10 which, for the period $t \in [5\text{ s}, 10\text{ s})$, is actuated but does not communicate with the other buses. Despite this, it can regulate its own bus voltage (compare this with the imperfect regulation with leaky integrators in Fig. 5).

Finally, the results in Fig. 11 show the steady-state bus voltages achieved before each change in Fig. 9. These values in color are contrasted with the steady state achieved when using a linear gain ($h_{\text{w}}(v_k) = v_k$) shown in gray. By using the nonlinear weighting function (29), the largest steady-state error over all nodes, $\max_k |v_{\text{Ref}} - \hat{v}_k|$, is between 1.7 and 2.4 V (at least 11.8%) smaller for the five steady-state sets in Fig. 11. Using the nonlinear weighting function, thus, allows a better regulation of the critical node voltages. We note that using the nonlinear weighting function increases[9] the variance of the steady-state voltage errors in Fig. 11. Nevertheless, the maximum voltage error has greater importance in dc networks compared to the voltage error variance since a smaller variance is meaningless if the voltage at one or more buses falls outside the tolerance band.

VIII. Conclusion

In this article, we proposed a four-stage distributed control structure that achieves power sharing in a dc microgrid while ensuring voltage regulation for the voltages of both actuated and unactuated buses. We demonstrated how the passivity properties of various subsystems can be determined and combined these to form sufficient conditions for the asymptotic stability for the controlled microgrid equilibrium manifold. These conditions are independent of topological changes, actuation changes, bus connections or disconnections, and load changes.

Future work includes the consideration of nonpassive loads at arbitrary locations in the microgrid and the construction of an interface to allow for the presented work to be combined with tertiary optimal controllers.

Appendix A
Proofs

Proof of Proposition 8: For the control structure in steady state, $\dot{\boldsymbol{x}}_{\text{u}} = 0$, and thus, $\boldsymbol{y}_{\text{u}}$ is constant. The steady-state output (25) of the Stage-4 DDA, therefore, ensures that Objective 2 is achieved. Furthermore, consider the steady state of the Stage-2 DDA

$$u_{\text{a},s,k} = \lim_{t\to\infty} h_{\text{w}}(v_{\text{Ref}} - v_k) \tag{65}$$

$$\lim_{t\to\infty} y_{\text{a},2,k} = \frac{\boldsymbol{u}_{\text{a},s}^{\text{T}} \mathbb{1}_N}{N} = \lim_{t\to\infty} \frac{1}{N} \sum_{k\in\mathcal{N}} (v_{\text{Ref}} - h(v_k)) \tag{66}$$

if v_k is in equilibrium and where h is obtained by shifting h_{w} by v_{Ref} such that $h(v_k) \coloneqq -h_{\text{w}}(v_{\text{Ref}} - v_k) + v_{\text{Ref}}$. Note that (66) corresponds to the condition of (22) in Objective 1. Therefore, $\boldsymbol{y}_{\text{a},2}$ specifies the regulation error of the average weighted voltage error in steady state. From the steady state of the agent PI controller in (27), we have $\zeta_{\text{u}}\boldsymbol{x}_{\text{u}} = \boldsymbol{y}_{\text{a},2}$. Thus, ideal integrators with $\zeta_{\text{u}} = 0$ ensure that Objective 1 is met exactly. For $\zeta_{\text{u}} > 0$, substitute the PI equilibrium into the output of the agent PI controller in (27) to obtain the steady-state equation

$$\boldsymbol{x}_{\text{u}} = \frac{1}{k_{\text{u}}^I} \left(\boldsymbol{y}_{\text{u}} + k_{\text{u}}^P \boldsymbol{y}_{\text{a},2} \right). \tag{67}$$

Substitute $\zeta_{\text{u}}\boldsymbol{x}_{\text{u}} = \boldsymbol{y}_{\text{a},2}$ into (25) and simplify to find

$$\boldsymbol{y}_{\text{a},2} = \frac{\zeta_{\text{u}}}{k_{\text{u}}^I \left(1 + \zeta_{\text{u}} k_{\text{u}}^P\right)} \boldsymbol{y}_{\text{u}} \tag{68}$$

[9]For example, the root mean square of the voltage error is 16.8 V for the linear and 18.1 V for the nonlinear function at $t = 19.95$ s.

for the steady state. Therefore, the steady-state output for the Stage-4 DDA in (25) gives $\boldsymbol{y}_{\mathrm{u}} = \boldsymbol{y}_{\mathrm{a},4}$, which we combine with (68) to obtain the error for Objective 1 in (31). ■

Proof of Theorem 14: Consider the supply rates which describe the actuated and unactuated states, respectively, for a given bus $k \in \mathcal{N}$

$$w_{\mathrm{M},\alpha,k} = (1+\nu_{\mathrm{d},1}\rho_{\mathrm{d}})\tilde{\phi}^*_{\alpha,k}\tilde{v}_{\alpha,k} - \nu_{\mathrm{d},1}\big(\tilde{\phi}^*_{\alpha,k}\big)^2 - \rho_{\mathrm{d}}\tilde{v}^2_{\alpha,k} \tag{69}$$

$$w_{\mathrm{M},\beta,k} = -\rho_{\mathrm{L}}\tilde{v}^2_{\beta,k}. \tag{70}$$

These allow the microgrid supply rate in (48) to be decomposed according to the actuation states α_k

$$\begin{aligned} w_{\mathrm{M},\alpha\beta} &= \sum_{k\in\mathcal{N}_\alpha} w_{\mathrm{M},\alpha,k} + \sum_{k\in\mathcal{N}_\beta} w_{\mathrm{M},\beta,k} \\ &= \sum_{k\in\mathcal{N}} \big(\alpha_k w_{\mathrm{M},\alpha,k} + (1-\alpha_k) w_{\mathrm{M},\beta,k}\big). \end{aligned} \tag{71}$$

Enlarge the supply rate of the unactuated buses in (70) by adding the positive term $\nu_{\mathrm{L}}(\tilde{\phi}^*_{\beta,k})^2$ for an arbitrarily small $\nu_{\mathrm{L}} > 0$ such that

$$\begin{aligned} w_{\mathrm{M},\beta,k} \le \overline{w}_{\mathrm{M},\beta,k} &= \nu_{\mathrm{L}}\big(\tilde{\phi}^*_{\beta,k}\big)^2 - \rho_{\mathrm{L}}\tilde{v}^2_{\beta,k} \\ \le \frac{\overline{w}_{\mathrm{M},\beta,k}}{\rho_{\mathrm{L}}} &= \frac{\nu_{\mathrm{L}}}{\rho_{\mathrm{L}}}\big(\tilde{\phi}^*_{\beta,k}\big)^2 - \tilde{v}^2_{\beta,k} \end{aligned} \tag{72}$$

for ρ_{L} as in (54). The supply rate $\overline{w}_{\mathrm{M},\beta,k}/\rho_{\mathrm{L}}$ is equivalent to the L_2 supply rate in Definition 2 and is, thus, bounded by the sector $[-(\nu_{\mathrm{L}}/\rho_{\mathrm{L}})^{1/2}, (\nu_{\mathrm{L}}/\rho_{\mathrm{L}})^{1/2}]$ [29, Lemma 4]. Consider now the supply rate of the actuated agents (69) narrowed down to an IFP sector for the case that $\rho_{\mathrm{d}} < 0$ and where the supply rate is unchanged otherwise. This gives

$$w_{\mathrm{M},\alpha,k} \ge \underline{w}_{\mathrm{M},\alpha,k} = \begin{cases} w_{\mathrm{M},\alpha,k}, & \text{if } \rho_{\mathrm{d}} \ge 0 \\ \tilde{\phi}^*_{\alpha,k}\tilde{v}_{\alpha,k} - \nu_{\mathrm{d},1}\big(\tilde{\phi}^*_{\alpha,k}\big)^2, & \text{if } \rho_{\mathrm{d}} < 0 \end{cases} \tag{73}$$

such that $\underline{w}_{\mathrm{M},\alpha,k}$ is sector bounded by $[\nu_{\mathrm{d},1}, (1/\rho_{\mathrm{d}})]$ if $\rho_{\mathrm{d}} > 0$ and $[\nu_{\mathrm{d},1}, \infty)$ if $\rho_{\mathrm{d}} < 0$ or if $\rho_{\mathrm{d}} = 0$ (see [26, p. 231]). A relation between $\underline{w}_{\mathrm{M},\alpha}$ and $\overline{w}_{\mathrm{M},\beta}/\rho_{\mathrm{L}}$ can now be established by comparing their respective sector bounds

$$\frac{\overline{w}_{\mathrm{M},\beta,k}}{\rho_{\mathrm{L}}} \le \underline{w}_{\mathrm{M},\alpha,k} \text{ if } \begin{cases} \left[-\sqrt{\frac{\nu_{\mathrm{L}}}{\rho_{\mathrm{L}}}}, \sqrt{\frac{\nu_{\mathrm{L}}}{\rho_{\mathrm{L}}}}\right] \subseteq \left[\nu_{\mathrm{d},1}, \frac{1}{\rho_{\mathrm{d}}}\right], \\ \qquad\qquad \text{if } \rho_{\mathrm{d}} > 0 \\ \left[-\sqrt{\frac{\nu_{\mathrm{L}}}{\rho_{\mathrm{L}}}}, \sqrt{\frac{\nu_{\mathrm{L}}}{\rho_{\mathrm{L}}}}\right] \subseteq [\nu_{\mathrm{d},1}, \infty), \\ \qquad\qquad \text{if } \rho_{\mathrm{d}} \le 0. \end{cases} \tag{74}$$

Since ν_{L} can be arbitrarily small, we derive (55) by comparing the lower bounds in (74) and note that the upper bound relation can be met for any ρ_{d}. A visual comparison of the sector conditions is made in Fig. 12. The combination of (72)–(74) results in

$$w_{\mathrm{M},\beta,k} \le \overline{w}_{\mathrm{M},\beta,k} \le \frac{\overline{w}_{\mathrm{M},\beta,k}}{\rho_{\mathrm{L}}} \le \underline{w}_{\mathrm{M},\alpha,k} \le w_{\mathrm{M},\alpha,k}. \tag{75}$$

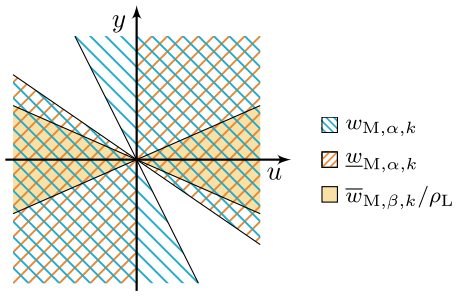

Fig. 12. Comparison of the microgrid supply rate sectors in the proof of Theorem 14 if $\rho_{\mathrm{d}} < 0$.

TABLE III
ROUNDED LINE LENGTHS

Line	Length	Line	Length	Line	Length
1 – 2	1.19 km	1 – 4	7.74 km	2 – 3	2.23 km
2 – 4	7.20 km	3 – 5	3.14 km	3 – 8	2.82 km
4 – 5	3.72 km	4 – 6	6.75 km	4 – 7	1.16 km
6 – 7	4.44 km	6 – 9	3.11 km	7 – 8	3.69 km
8 – 10	1.21 km				

TABLE IV
STRICTLY PASSIVE LOAD VALUES

Bus	Parameter	$t = 0$ s	$t = 5$ s	$t = 10$ s	$t = 15$ s	$t = 20$ s
1	Z^{-1} (1/Ω)	0.103	0.103	0.106	0.106	0.083
	I (A)	4.66	2.15	-6.08	-6.08	14.45
	P (W)	3599	-4055	4133	4133	-4927
2	Z^{-1} (1/Ω)	0.099	0.099	0.096	0.096	0.080
	I (A)	-16.09	-16.09	19.68	19.68	2.49
	P (W)	3204	3204	2659	2659	1346
3	Z^{-1} (1/Ω)	0.128	0.105	0.105	0.105	0.096
	I (A)	10.27	-0.09	-0.09	-0.09	-11.09
	P (W)	-1479	-3659	-3659	-3659	3031
4	Z^{-1} (1/Ω)	0.079	0.079	0.079	0.079	0.079
	I (A)	10.15	10.15	10.15	10.15	10.15
	P (W)	-2711	-2711	-2711	-2711	-2711
5	Z^{-1} (1/Ω)	0.095	0.095	0.095	0.064	0.107
	I (A)	-6.64	-6.64	-6.64	16.68	2.10
	P (W)	2768	2768	2768	-3798	4242
6	Z^{-1} (1/Ω)	0.089	0.089	0.106	0.103	0.103
	I (A)	6.87	6.87	7.85	-5.17	-5.17
	P (W)	948	948	4321	370	370
7	Z^{-1} (1/Ω)	0.065	0.092	0.092	0.118	0.118
	I (A)	11.96	6.51	6.51	2.77	2.77
	P (W)	-3624	-3442	-3442	-3890	-3890
8	Z^{-1} (1/Ω)	0.102	0.102	0.086	0.086	0.124
	I (A)	-16.85	-16.85	20.71	20.71	-4.68
	P (W)	3529	3529	-4773	-4773	-3832
9	Z^{-1} (1/Ω)	0.111	0.103	0.109	0.077	0.077
	I (A)	13.79	-19.74	9.53	1.26	1.26
	P (W)	-2645	1830	4215	1549	1549
10	Z^{-1} (1/Ω)	0.072	0.100	0.100	0.111	0.111
	I (A)	7.77	9.02	9.02	10.98	10.98
	P (W)	-3538	-4143	-4143	-2795	-2795

Therefore, for the microgrid with the storage function S_{M} (50) that is dissipative with respect to (48), it holds that

$$\begin{aligned} \dot{S}_{\mathrm{M}} \le w_{\mathrm{M},\alpha\beta} &\le \sum_{k\in\mathcal{N}} \big(\alpha_k w_{\mathrm{M},\alpha,k} + (1-\alpha_k) w_{\mathrm{M},\alpha,k}\big) \\ &= \sum_{k\in\mathcal{N}} w_{\mathrm{M},\alpha,k} = w_{\mathrm{M}} \end{aligned} \tag{76}$$

which is found by combining (71) with (75). ■

TABLE V
PASSIVE LOAD VALUES, WITH P AS IN TABLE IV

Bus	Parameter	$t = 0\,\mathrm{s}$	$t = 5\,\mathrm{s}$	$t = 10\,\mathrm{s}$	$t = 15\,\mathrm{s}$	$t = 20\,\mathrm{s}$
1	Z^{-1} $(1/\Omega)$	0.091	0.093	0.087	0.087	0.063
	I (A)	4.66	-8.15	-6.08	-6.08	9.71
2	Z^{-1} $(1/\Omega)$	0.069	0.069	0.071	0.071	0.046
	I (A)	-16.09	-16.09	19.68	19.68	0.20
3	Z^{-1} $(1/\Omega)$	0.095	0.082	0.082	0.082	0.059
	I (A)	8.91	-7.12	-7.12	-7.12	-11.09
4	Z^{-1} $(1/\Omega)$	0.038	0.038	0.038	0.038	0.038
	I (A)	8.82	8.82	8.82	8.82	8.82
5	Z^{-1} $(1/\Omega)$	0.065	0.065	0.065	0.027	0.078
	I (A)	-6.64	-6.64	-6.64	15.25	2.10
6	Z^{-1} $(1/\Omega)$	0.071	0.071	0.089	0.102	0.102
	I (A)	4.04	4.04	7.85	-9.19	-9.19
7	Z^{-1} $(1/\Omega)$	0.029	0.070	0.070	0.079	0.079
	I (A)	9.04	0.89	0.89	0.58	0.58
8	Z^{-1} $(1/\Omega)$	0.075	0.075	0.057	0.057	0.111
	I (A)	-16.85	-16.85	20.55	20.55	-14.31
9	Z^{-1} $(1/\Omega)$	0.105	0.102	0.061	0.036	0.036
	I (A)	10.71	-19.75	9.53	-0.05	-0.05
10	Z^{-1} $(1/\Omega)$	0.042	0.091	0.091	0.088	0.088
	I (A)	2.53	2.03	2.03	8.34	8.34

APPENDIX B
SIMULATION DATA

The simulation parameters used for the lines in Section VII are given in Table III. Furthermore, the strictly passive load parameters for the simulation results in Section VII-B and the passive load parameters for the results in Section VII-C are given in Tables IV and V, respectively. Note that the P parameter for the loads in Table V are the same as listed in Table IV.

REFERENCES

[1] B. Lasseter, "Microgrids [distributed power generation]," in *Proc. IEEE Power Eng. Soc. Winter Meeting Conf.*, vol. 1, Jan./Feb. 2001, pp. 146–149.

[2] J. J. Justo, F. Mwasilu, J. Lee, and J.-W. Jung, "AC-microgrids versus DC-microgrids with distributed energy resources: A review," *Renew. Sustain. Energy Rev.*, vol. 24, pp. 387–405, Aug. 2013.

[3] L. Meng et al., "Review on control of DC microgrids and multiple microgrid clusters," *IEEE J. Emerg. Sel. Topics Power Electron.*, vol. 5, no. 3, pp. 928–948, Sep. 2017.

[4] V. Nasirian, S. Moayedi, A. Davoudi, and F. L. Lewis, "Distributed cooperative control of DC microgrids," *IEEE Trans. Power Electron.*, vol. 30, no. 4, pp. 2288–2303, Apr. 2015.

[5] M. Tucci, L. Meng, J. M. Guerrero, and G. Ferrari-Trecate, "Stable current sharing and voltage balancing in DC microgrids: A consensus-based secondary control layer," *Automatica*, vol. 95, pp. 1–13, Sep. 2018.

[6] J. Zhao and F. Dörfler, "Distributed control and optimization in DC microgrids," *Automatica*, vol. 61, pp. 18–26, Nov. 2015.

[7] T. Dragicevic, X. Lu, J. C. Vasquez, and J. M. Guerrero, "DC microgrids—Part I: A review of control strategies and stabilization techniques," *IEEE Trans. Power Electron.*, vol. 31, no. 7, pp. 4876–4891, Jul. 2016.

[8] J. Kumar, A. Agarwal, and V. Agarwal, "A review on overall control of DC microgrids," *J. Energy Storage*, vol. 21, pp. 113–138, Feb. 2019.

[9] M. Tucci, S. Riverso, J. C. Vasquez, J. M. Guerrero, and G. Ferrari-Trecate, "A decentralized scalable approach to voltage control of DC islanded microgrids," *IEEE Trans. Control Syst. Technol.*, vol. 24, no. 6, pp. 1965–1979, Nov. 2016.

[10] F. Strehle, M. Pfeifer, A. J. Malan, S. Krebs, and S. Hohmann, "A scalable port-Hamiltonian approach to Plug-and-Play voltage stabilization in DC microgrids," in *Proc. IEEE Conf. Control Technol. Appl. (CCTA)*, Aug. 2020, pp. 787–794.

[11] M. Cucuzzella, K. C. Kosaraju, and J. M. A. Scherpen, "Voltage control of DC microgrids: Robustness for unknown ZIP-loads," *IEEE Control Syst. Lett.*, vol. 7, pp. 139–144, 2023.

[12] S. Trip, M. Cucuzzella, X. Cheng, and J. Scherpen, "Distributed averaging control for voltage regulation and current sharing in DC microgrids," *IEEE Control Syst. Lett.*, vol. 3, no. 1, pp. 174–179, Jan. 2019.

[13] M. Cucuzzella, S. Trip, C. De Persis, X. Cheng, A. Ferrara, and A. J. van der Schaft, "A robust consensus algorithm for current sharing and voltage regulation in DC microgrids," *IEEE Trans. Control Syst. Technol.*, vol. 27, no. 4, pp. 1583–1595, Jul. 2019.

[14] M. S. Sadabadi, S. Sahoo, and F. Blaabjerg, "Stability-oriented design of cyberattack-resilient controllers for cooperative DC microgrids," *IEEE Trans. Power Electron.*, vol. 37, no. 2, pp. 1310–1321, Feb. 2022.

[15] R. Han, L. Meng, J. M. Guerrero, and J. C. Vasquez, "Distributed nonlinear control with event-triggered communication to achieve current-sharing and voltage regulation in DC microgrids," *IEEE Trans. Power Electron.*, vol. 33, no. 7, pp. 6416–6433, Jul. 2018.

[16] P. Nahata and G. Ferrari-Trecate, "On existence of equilibria, voltage balancing, and current sharing in consensus-based DC microgrids," in *Proc. Eur. Control Conf. (ECC)*, May 2020, pp. 1216–1223.

[17] P. Nahata, M. S. Turan, and G. Ferrari-Trecate, "Consensus-based current sharing and voltage balancing in DC microgrids with exponential loads," *IEEE Trans. Control Syst. Technol.*, vol. 30, no. 4, pp. 1668–1680, Jul. 2022.

[18] C. De Persis, E. R. A. Weitenberg, and F. Dörfler, "A power consensus algorithm for DC microgrids," *Automatica*, vol. 89, pp. 364–375, Mar. 2018.

[19] B. Fan, S. Guo, J. Peng, Q. Yang, W. Liu, and L. Liu, "A consensus-based algorithm for power sharing and voltage regulation in DC microgrids," *IEEE Trans. Ind. Informat.*, vol. 16, no. 6, pp. 3987–3996, Jun. 2020.

[20] M. Cucuzzella, K. C. Kosaraju, and J. M. A. Scherpen, "Distributed passivity-based control of DC microgrids," in *Proc. Amer. Control Conf. (ACC)*, Jul. 2019, pp. 652–657.

[21] F. Dörfler and F. Bullo, "Kron reduction of graphs with applications to electrical networks," *IEEE Trans. Circuits Syst. I, Reg. Papers*, vol. 60, no. 1, pp. 150–163, Jan. 2013.

[22] W. Chen et al., "On spectral properties of signed Laplacians with connections to eventual positivity," *IEEE Trans. Autom. Control*, vol. 66, no. 5, pp. 2177–2190, May 2021.

[23] A. J. Malan, M. Pfeifer, and S. Hohmann, "Distributed coordination of physically-interconnected multi-agent systems with actuated and unactuated agents," *Eur. J. Control*, vol. 68, Nov. 2022, Art. no. 100673.

[24] A. J. van der Schaft, *L2-Gain Passivity Techn. Nonlinear Control*, 3rd ed. Cham, Switzerland: Springer, 2017.

[25] M. Arcak and E. D. Sontag, "Diagonal stability of a class of cyclic systems and its connection with the secant criterion," *Automatica*, vol. 42, no. 9, pp. 1531–1537, Sep. 2006.

[26] H. K. Khalil, *Nonlinear Systems*, 3rd ed. Upper Saddle River, NJ, USA: Prentice-Hall, 2002.

[27] G. H. Hines, M. Arcak, and A. K. Packard, "Equilibrium-independent passivity: A new definition and numerical certification," *Automatica*, vol. 47, no. 9, pp. 1949–1956, 2011.

[28] M. Arcak, C. Meissen, and A. Packard, *Networks of Dissipative Systems: Compositional Certification of Stability, Performance, and Safety* (Springer Briefs in Control, Automation and Robotics). New York, NY, USA: Springer, 2016.

[29] A. J. Malan, P. Jané-Soneira, and S. Hohmann, "Constructive analysis and design of interconnected Krasovskii passive and quadratic dissipative systems," in *Proc. IEEE 61st Conf. Decis. Control (CDC)*, Dec. 2022, pp. 7059–7065.

[30] P. Moylan and D. Hill, "Stability criteria for large-scale systems," *IEEE Trans. Autom. Control*, vol. AC-23, no. 2, pp. 143–149, Apr. 1978.

[31] M. Benzi, G. H. Golub, and J. Liesen, "Numerical solution of saddle point problems," *Acta Numerica*, vol. 14, pp. 1–137, May 2005.

[32] F. Strehle, A. J. Malan, S. Krebs, and S. Hohmann, "Passivity conditions for plug-and-play operation of nonlinear static AC loads," *IFAC-PapersOnLine*, vol. 53, no. 2, pp. 12237–12243, 2020.

[33] J. Machowski, J. W. Bialek, and J. R. Bumby, *Power System Dynamics: Stability and Control*, 2nd ed. Chichester, U.K.: Wiley, 2008.

[34] R. A. Freeman, P. Yang, and K. M. Lynch, "Stability and convergence properties of dynamic average consensus estimators," in *Proc. 45th IEEE Conf. Decis. Control*, San Diego, CA, USA, Dec. 2006, pp. 338–343.

[35] E. Weitenberg, Y. Jiang, C. Zhao, E. Mallada, F. Dörfler, and C. De Persis, "Robust decentralized frequency control: A leaky integrator approach," in *Proc. Eur. Control Conf. (ECC)*, Jun. 2018, pp. 764–769.

[36] T. Raff, C. Ebenbauer, and F. Allgöwer, *Nonlinear Model Predictive Control: A Passivity-Based Approach*. Berlin, Germany: Springer, 2007, pp. 151–162.

Albertus Johannes Malan received the B.Eng. degree in electronic engineering from the University of Pretoria, Pretoria, South Africa, in 2015, and the M.Sc. degree in electrical engineering and information technology from the Karlsruhe Institute of Technology (KIT), Karlsruhe, Germany, in 2019, where he is currently pursuing the Ph.D. degree in control engineering with the Institute of Control Systems (IRS).

His research interests include multi-agent systems, passivity-based stability, and the control of networked multi-energy systems.

Pol Jané-Soneira (Graduate Student Member, IEEE) received the B.Sc. and M.Sc. degrees in electrical engineering and information technology from the Karlsruhe Institute of Technology (KIT), Karlsruhe, Germany, in 2016 and 2019, respectively, where he is currently pursuing the Ph.D. degree in control engineering with the Institute of Control Systems (IRS).

His main research interests are optimal control theory, distributed optimization, and model predictive control with applications to networked energy systems.

Felix Strehle received the B.Sc. and M.Sc. degrees in electrical engineering and information technology and the Ph.D. degree in control engineering from the Karlsruhe Institute of Technology (KIT), Karlsruhe, Germany, in 2015, 2017, and 2024, respectively.

Since June 2022, he has been leading the research group on networked multi-energy systems with the Institute of Control Systems (IRS), KIT. His main research interests are centered around energy-based modeling and decentralized, passivity-based control, and stability with application to networked multi-energy systems, such as power systems, microgrids, district heating networks, gas networks, and integrated combinations thereof.

Sören Hohmann (Member, IEEE) received the Diploma and Ph.D. degrees from the University of Karlsruhe, Karlsruhe, Germany, in 1997 and 2002, respectively.

He studied electrical engineering jointly with the Technische Universität Braunschweig, Brunswick, Germany; the University of Karlsruhe; and the École Nationale Supérieure d'Électricité et de Mécanique, Nancy, France. Afterward, until 2010, he worked with the industry for BMW, Munich, Germany, where his last position was the Head of the predevelopment and series development of active safety systems. He is currently the Head of the Institute of Control Systems (IRS), Karlsruhe Institute of Technology (KIT), Karlsruhe, and a Director's Board Member of the Research Center for Information Technology (FZI), Karlsruhe. His research interests are cooperative control, networked multi-energy systems, and system guarantees by design.